# Microscopic diagnosis of universal geometric responses in fractional quantum Hall liquids

Liangdong Hu, Zhao Liu, D. N. Sheng, F. D. M. Haldane, and W. Zhu

Phys. Rev. B **103**, 085103 — Published 2 February 2021

DOI: 10.1103/PhysRevB.103.085103

# Microscopic Diagnosis of Universal Geometric Responses in Fractional Quantum Hall Liquids

Liangdong Hu[1], Zhao Liu[2], and D. N. Sheng[3], F. D. M. Haldane[4], W. Zhu[1,†]
[1] *Westlake Institute of Advanced Study, Westlake University, Hangzhou, 310024, China*
[2]*Zhejiang Institute of Modern Physics, Zhejiang University, Hangzhou 310027, China*
[3]*Department of Physics and Astronomy, California State University, Northridge, CA 91330, USA and*
[4]*Department of Physics, Princeton University, Princeton, New Jersey 08544, USA*[*]
(Dated: January 12, 2021)

Topological quantum liquids contain internal degrees of freedom that are coupled to geometric response. Yet, an explicit and microscopic identification of the geometric response remains difficult. Here, taking notable fractional quantum Hall (FQH) states as typical examples, we systematically investigate a promising protocol – the Dehn twist deformation on the torus geometry, to probe the geometric response of correlated topological states and establish the relation between such response and universal properties of pertinent states. Based on analytical derivations and numerical simulations, we find that the geometry-induced Berry phase encodes novel features for a broad class of FQH states at the Laughlin, hierarchy, Halperin and non-Abelian Moore-Read fillings. Our findings conclusively demonstrate that the adiabatic Dehn twist deformation can faithfully capture rich geometric and topological information, including the Hall viscosity and topological spin of the pertinent FQH state and the chiral central charge of the underlying edge conformal field theory. Our approach provides a powerful way to reveal topological orders of generic FQH states and address previously open questions.

## I. INTRODUCTION

Topological phases of matter[1] possess a variety of properties which are robust against external perturbations as long as the topology of space where the system is defined is not altered. As a celebrated example, the fractional quantum Hall (FQH) effect[2] formed by two-dimensional interacting particles in strong magnetic fields has attracted broad interest in the past decades. The topologically invariant properties of FQH states, including the quantized electrical[3–5] and thermal Hall conductances[6–8], topological ground-state degeneracies[9], exotic anyonic quasiparticles[10–12], and entanglement characteristics[13–15], have been extensively studied from both theoretical and experimental sides.

Despite FQH states are often characterized by their topologically invariant features, these states do have intriguing response to variations of the ambient geometry even if these variations preserve the underlying topology. Two representative examples are the intrinsic "orbital spin" [16–18] and the Hall viscosity[17,19–21]. The former can be related to intrinsic metrics which describe deformations of an FQH droplet due to anisotropies in the background space (for instance those induced by tilted or spatially inhomogeneous magnetic fields[22,23]), while the latter determines a Berry phase caused by strains applied to the FQH droplet[19,20]. Moreover, transport coefficients of FQH states can also be understood as a response to variations of spatial geometry[24–27]. As the geometric response is closely related to the internal topological structure of FQH liquids, it provides an ideal platform to study the interplay between geometry and topology in FQH liquids.

Nevertheless, so far most studies about the geometric response heavily relied on effective field theories[16,20,28–38] and model wave functions[39–43]. A recent progress has been made in microscopic models to connect the topological contents of FQH states encoded in modular $\mathcal{T}$-transformation (or Dehn twist) operation[44–46] to the momentum polarization via the entanglement spectra[47,48]. However, a direct microscopic investigation of the evolution of generic FQH wave functions themselves with variations of the ambient geometry is still lacking.

In this work, we aim to fill in this blank by explicitly implementing the Dehn twist on the torus, tracking the evolution of FQH wave functions, and establishing the relation between the geometric response of FQH states and their universal (topological and geometric) properties. Instead of relying on physical arguments, this relation is analytically derived under a gauge-fixing scheme for model FQH wave functions, and can be readily confirmed by numerical simulations in microscopic models for generic FQH states. Our main finding is, for a robust FQH phase with a set of degenerate ground states evolving adiabatically during the Dehn twist, there is an accumulated Berry phase in each ground state which contains both topological and geometric information: the Hall viscosity related to the guiding-center spin[18,20,41], the sector-dependent topological spin[47,48], and the chiral central charge of the underlying edge conformal field theory (CFT). These information fully characterizes the underlying topological order. By using extensive exact diagonalization to track the evolution of ground-state wave functions and calculate the accumulated Berry phase, we demonstrate the validity of this relation for various FQH states at the fermionic and bosonic Laughlin, hierarchy, Halperin and non-Abelian Moore-Read fillings, and successfully extract the topological and geometric properties of both model wave functions and Coulomb ground states. As a byproduct, we find that the flow of energy spectra under geometric deformation plays as a "smoking-gun" feature to justify the robustness of FQH liquids. In this context, we demonstrate that the ground-state degeneracy at $\nu = 5/2$ under particle-hole symmetric interactions is fragile, which challenges the identification of (anti-)Pfaffian state based on finite-size calculations.

## II. GEOMETRIC BERRY PHASE FROM DEHN TWIST

We consider $N_p$ particles with charge $e$ moving in two spatial dimensions on the torus geometry subjected to a perpen-

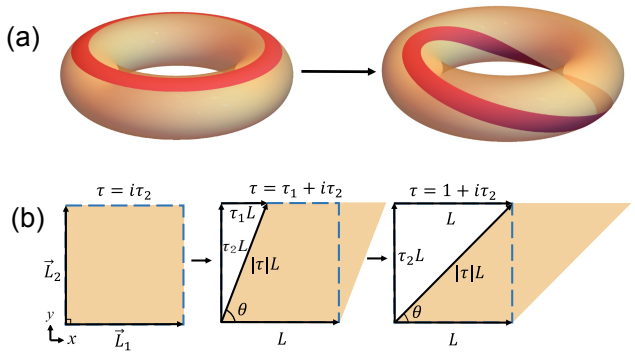


FIG. 1. **Dehn twist operation on the torus.** (a) A twist operation on the annulus (red) illustrates the self-homeomorphism of $\mathcal{T}$ transformation. (b) The torus geometry is defined by two fundamental vectors $\vec{L}_2 = L\vec{\tau}$ and $\vec{L}_1 = L\vec{e}_x$, and the twist angle is $\theta$. The Dehn twist, i.e., the $\mathcal{T}$ transformation sends $\vec{\tau} = \tau_1\vec{e}_x + \tau_2\vec{e}_y$ to its equivalent geometry $\vec{\tau}+\vec{e}_x$, thus leaves the torus geometry unchanged. The area of the torus does not change during the Dehn twist. Here we give an example of the Dehn twist changing $\vec{\tau}$ from $\tau_2\vec{e}_y$ to $\vec{e}_x + \tau_2\vec{e}_y$, with $\tau_2 = |\vec{L}_2(\theta = \pi/2)|/|\vec{L}_1|$.

dicular uniform magnetic field. The torus is spanned by two vectors $\vec{L}_1 = L\vec{e}_x$ and $\vec{L}_2 = L\vec{\tau}$[49], where $\vec{\tau}$ is parametrized by the twist angle $\theta$ as $\vec{\tau} = \tau_1\vec{e}_x + \tau_2\vec{e}_y = (\cos\theta\vec{e}_x + \sin\theta\vec{e}_y)|\vec{L}_2|/|\vec{L}_1|$ such that $\vec{L}_2 = \vec{L}_2(\theta)$ depends on $\theta$ (Fig. 1). Here $\vec{e}_x$ and $\vec{e}_y$ are unit vectors in the $x$ and $y$ directions, respectively. After rephrasing the coordinate $x\vec{e}_x + y\vec{e}_y$ as $L(X^1\vec{e}_x + X^2\vec{\tau})$ with $X^1, X^2 \in [0, 1]$, we can express the single-particle Hamiltonian as

$$H_0(\tau) = \frac{1}{2}g^{ab}(\tau)D_a(\mathbf{A})D_b(\mathbf{A}) \tag{1}$$

with

$$g(\tau) = \frac{1}{L^2\tau_2^2}\begin{pmatrix} |\tau|^2 & -\tau_1 \\ -\tau_1 & 1 \end{pmatrix}, \tag{2}$$

where the vector potential $\mathbf{A} = -\tau_2 LBX^2\vec{e}_x$, and the covariant derivative $D_a(\mathbf{A}) = -i\hbar\partial/\partial X^a + |e|A_a$. The inverse-mass-matrix (also called Riemann metric) $g(\tau)$ depends on the shape of the torus, which plays the role of a geometric metric[20,21,38,39,50–52]. The total number of fluxes $N_\phi$ penetrating the torus is given by the Landau level degeneracy $N_\phi = |\vec{L}_1 \times \vec{L}_2|/(2\pi\ell^2)$, where the magnetic length $\ell = \sqrt{\hbar/(|e|B)}$ is taken as the length unit. The filling factor is defined as $\nu = N_p/N_\phi$.

We focus on the continuous geometric deformation generated by the Dehn twist operation on the torus, which corresponds to the adiabatic process $\vec{\tau} \to \vec{\tau} + \vec{e}_x$ as illustrated in Fig. 1. Since the torus geometry after Dehn twist is equivalent to the original one, the physics of a topological order should be left unchanged[5]. As required by the principle of gauge invariance, we expect that the nearly degenerate ground-state manifold of a stable FQH phase should evolve adiabatically in the whole process of Dehn twist, and each ground state should finally acquire a sector-dependent Berry phase. One advantage of our choice of Dehn twist is the potentially rich information contained in these Berry phases. First, the process of Dehn twist operation is equivalent to shearing the torus geometry, which is similar to applying a strain to a fluid. As a result, these Berry phases should reflect the viscosity response of FQH states[19,20,39]. Second, the Dehn twist operation coincides with the $\mathcal{T}$-transformation in the 1+1D CFT[44] describing the edge of the underlying FQH state, thus we expect to extract the topological properties of modular tensor category of the pertinent state from these Berry phases[43,45,53,54]. Third, the adiabatic evolution of the FQH ground-state manifold itself can be used as a criterion for the robustness of FQH liquids, which so far has not been confirmed by proof-of-principle numerical evidence.

### A. Geometric phase

In order to explicitly illustrate the Dehn-twist induced Berry phase, we first consider the $\nu = 1/q$ Laughlin wave function in the topological sector $\alpha$ on the torus[10,46]:

$$\langle\{z_i\}|\Psi^\alpha;\tau\rangle = \mathcal{N}(\tau)\prod_{i<j}\left[\frac{\theta_{11}(z_i - z_j|\tau)}{\eta(\tau)}\right]^q \times f_c^\alpha\left(\{Z\}|\tau\right)e^{i\pi N_\phi\tau\sum_i[X_{2,i}]^2}, \tag{3}$$

where $z_i = x_i + iy_i$ is the coordinate of the $i$th particle. $\alpha$ labels the $q$ degenerate Laughlin states, each of which corresponds to a fixed type of quasiparticle. The center-of-mass part of the wave function is described by $f_c(\{Z\})$, the relative part is captured by the Jacobi-theta function $\theta_{11}(z_i - z_j|\tau)$, and the normalization prefactor $\mathcal{N}(\tau) = N_0[\sqrt{\tau_2}\eta^2(\tau)]^{N_\phi/2}$ with $N_0$ a $\tau$-independent constant and $\eta$ the Dedekind's function. The details of this wave function will be given in the Appendix Sec. A 3.

For the Laughlin wave function Eq. (3), we can analytically prove that, up to an $N_p$-dependent term which can be removed by a gauge transform, the Dehn-twist induced Berry phase is

$$U_\alpha^{\mathcal{T}} = -\eta^H L^2 + 2\pi h_\alpha - 2\pi\frac{c}{24}, \tag{4}$$

where $\eta^H$ is the Hall viscosity[19,20], $h_\alpha$ is the topological spin characterizing the adiabatic self-rotation of quasiparticle $\alpha$[47,48], and $c$ is the chiral central charge of the edge CFT of the underlying FQH state. We will give the proof of Eq. (4) in the Appendix Secs. A 4 and A 5, in which we find the Dehn twist induced Berry phase for general multicomponent Halperin model wave functions[55] takes the same form. As we will discuss below, the first term in Eq. (4) comes from the stress response to the deformation of torus, while the second and third terms are results of the response to the modular transform accompanying the Dehn twist.

### B. Hall viscosity response

The first term in Eq. (4) depends on the Hall viscosity $\eta^H$ and the length $L$ of the twist path. This term comes from the stress response, which is generally nonzero for time-reversal symmetry breaking Hall liquids[20,21,38,50–52]. For an FQH state at filling $\nu = p/q$, we can calculate the Berry connection resulting from the deformation of torus during the Dehn twist as (see Appendix Sec. A 5, where we use $p$ and $q$ to represent the numerator and denominator of filling factor $\nu = p/q$)

$$\mathcal{A}_\tau = i\langle\Psi;\bar{\tau}|\partial_\tau|\Psi;\tau\rangle = -\frac{qN_p}{8\tau_2}, \tag{5}$$

which is $\alpha$-independent and gives an accumulated Berry phase[19]

$$\int_0^1 \mathcal{A}_{\tau_1}\mathrm{d}\tau_1 = \int_0^1 (\mathcal{A}_\tau + \mathcal{A}_{\bar{\tau}})\mathrm{d}\tau_1 = -\frac{qN_p}{4\tau_2} = -\hbar^{-1}\eta^H L^2. \tag{6}$$

Microscopic studies of the FQH physics often project the whole system to the single partially filled Landau level for high numerical efficiency. In this case, $\eta^H$ in the Berry phase should be replaced by $\eta^g$, the so called guiding-center viscosity[17]. $\eta^g$ is related to the guiding-center spin $s$ of the underlying FQH state via $\eta^g = -\frac{\hbar}{4\pi\ell^2}\frac{s}{q}$, where $s$ describes an emergent geometric response of a correlated composite boson (with $p$ particles in consecutive $q$ orbitals) and can be used as a topological quantum number to distinguish different FQH states[18,20,41] (see more details in Appendix Sec. D).

### C. Modular response

Apart from tilting the torus, the Dehn twist, equivalently, the $\mathcal{T}$-transformation, is expected to encode topological information of the modular group on the torus[45,46]. Starting from Eq. (3), we can prove (see details in Appendix Sec. A 4)

$$\langle\{z_i\}|\Psi^\alpha;\tau+1\rangle = \langle\{z_i\}|\Psi^\alpha;\tau\rangle e^{2\pi i(h_\alpha - \frac{c}{24})} e^{i\frac{\pi q N_p^2}{12}}, \tag{7}$$

which leads to a Berry phase $2\pi(h_\alpha - \frac{c}{24}) + \frac{\pi q N_p^2}{12}$ in addition to the one purely caused by the torus deformation [Eq. (6)]. The matrix representation of $\mathcal{T}$ under the basis of initial states is thus

$$\langle\Psi^\beta;\tau|\mathcal{T}|\Psi^\alpha;\tau\rangle = \langle\Psi^\beta;\tau|\Psi^\alpha;\tau+1\rangle = T_{\alpha\beta}e^{i\gamma} \tag{8}$$

with

$$T_{\alpha\beta} = \delta_{\alpha\beta}e^{i2\pi(h_\alpha - \frac{c}{24})}, \tag{9}$$

which recovers the modular $T$-matrix, indicating that the overlap between microscopic ground-state wave functions before and after the Dehn twist can characterize the underlying topological phase[45,53,54]. Note that we have properly fixed the gauge in $|\Psi^\alpha;\tau\rangle$ and $|\Psi^\alpha;\tau+1\rangle$ to derive Eq. (8) (see Appendix Sec. A 4).

Beside the universal topological information $2\pi(h_\alpha - \frac{c}{24})$, there is an extra system-size-dependent phase factor

$$\gamma = \frac{\pi q N_p^2}{12} \tag{10}$$

in Eq. (8), which was overlooked in earlier studies[47]. However, it is necessary to isolate this non-universal term from the universal ones if we want to determine the topological spin and central charge from the microscopic simulation of Dehn twist[56].

## III. MICROSCOPIC MODEL

We aim to simulate the Dehn-twist-driven evolution of an FQH system with a translation-invariant two-body interaction projected to the lowest Landau level (LLL). The system is described by the Hamiltonian

$$H(\tau) = \frac{1}{2L_1L_2\sin\theta}\sum_{\mathbf{q}} V_{\mathbf{q}} :\hat{\rho}_{-\mathbf{q}}\hat{\rho}_{\mathbf{q}}: \tag{11}$$

where $V_{\mathbf{q}}$ is the Fourier transform of the interaction potential and $\hat{\rho}_{\mathbf{q}}$ is the LLL-projected density operator. The standard second quantization procedure gives

$$\hat{\rho}_{\mathbf{q}} = \int \mathrm{d}\mathbf{r}\, e^{-i\mathbf{q}\cdot\mathbf{r}} \sum_{j_1,j_2} \psi^*_{j_1}(\mathbf{r})\psi_{j_2}(\mathbf{r}) a^\dagger_{j_1}a_{j_2}, \tag{12}$$

where $a^\dagger_j$ creates a particle in LLL orbital $j$ ($j = 0,1,\cdots,N_\phi-1$), with wave function $\psi_j(x,y) = \left(\frac{1}{\pi^{1/2}L\ell}\right)^{1/2}\sum_k e^{2\pi(j+kN_\phi)\frac{x+iy}{L}+i\frac{\pi\tau}{N_\phi}(j+kN_\phi)^2}e^{-\frac{y^2}{2\ell^2}}$. In the following, we choose the Coulomb interaction with $V_{\mathbf{q}} = \frac{2\pi}{|\mathbf{q}|}$ or Haldane's pseudopotentials[57]. At filling $\nu = p/q$ with coprime $p$ and $q$, the full many-body symmetry can be factorized into a center-of-mass and a relative part[58,59], thus each eigenstate of Eq. (11) can be labeled by a two-dimensional momentum $\mathbf{K} = (K_1, K_2)$ with $K_{1,2} = 0,1,\cdots,N_\phi/q-1$ (equivalently, by $\mathbf{k} = (k_1,k_2)$ with $k_1 = 2\pi K_1/N_\phi$ and $k_2 = 2\pi K_2/(N_\phi/q)$) in the irreducible Brillouin zone.

### A. Dehn twist simulation

To simulate the Dehn twist, we parametrize the whole process in Fig. 1(b) by the twist angle $\theta$ of the torus which varies from $\pi/2$ to $\tan^{-1}(|\vec{L}_2(\theta=\pi/2)|/|\vec{L}_1|)$. We divide the path of $\theta$ into $M$ evenly spaced steps, and use exact diagonalization in the Fock basis of LLL orbitals to calculate the energy spectrum and eigenstates of Eq. (11) at each step. The accumulated Berry phase in topological sector $a$ can then be evaluated by the discretized formula[39,40]

$$e^{iU_a^{\mathcal{T}}} \simeq \langle\Psi_a(0)|\hat{U}_g|\Psi_a(M-1)\rangle \prod_{j=0}^{M-2}\langle\Psi_a(j+1)|\Psi_a(j)\rangle, \tag{13}$$

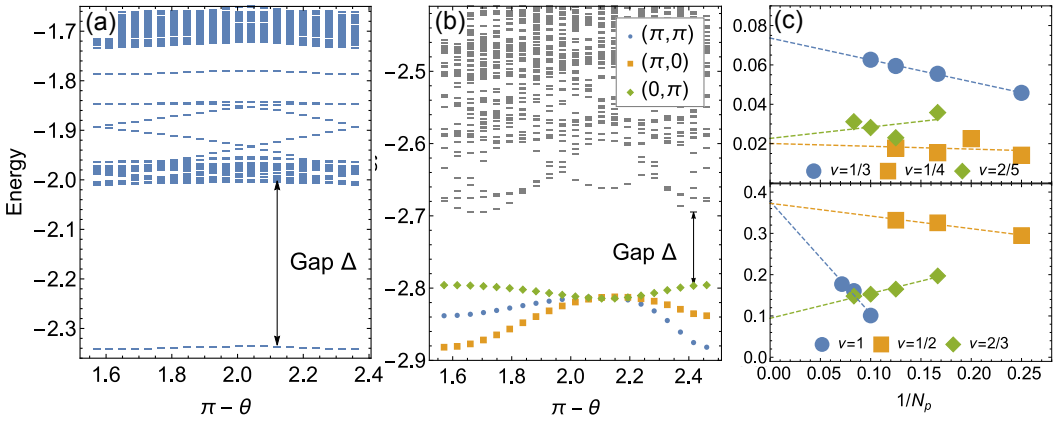


FIG. 2. **Flow of low-energy spectra.** The low-energy spectra of the Coulomb interaction as a function of the twist angle $\theta$ for (a) bosons at $\nu = 1/2$ with $N_p = 8$ and (b) bosons at $\nu = 1$ with $N_p = 12$. The initial geometric conditions before the Dehn twist are chosen as $|\vec{L}_1| = |\vec{L}_2|$ in (a) and $|\vec{L}_1| = 1.23|\vec{L}_2|$ in (b), with $\theta = \pi/2$. The spectra are calculated in the irreducible Brillouin zone $(K_1, K_2)$ with $K_{1,2} = 0, 1, ..., N_\phi/q - 1$. (c) Finite-size scaling of the minimal energy gap $\Delta$ during the Dehn twist for the $\nu = 1/2, 1/3, 1/4$ Laughlin states, $\nu = 2/5, 2/3$ hierarchy states and $\nu = 1$ Moore-Read state. The arrows in (a) and (b) indicate the minimal gap during the Dehn twist.

where $|\Psi_a(j)\rangle$ is the ground state in topological sector $a$ at step $j$, and $j = 0$ and $j = M$ correspond $\theta = \pi/2$ and $\theta = \tan^{-1}(|\vec{L}_2(\theta = \pi/2)|/|\vec{L}_1|)$, respectively. Note that the final state $|\Psi_a(M)\rangle$ in Eq. (13) is not calculated by diagonalizing the Hamiltonian, but is directly transformed from the initial state $|\Psi_a(0)\rangle$ by $|\Psi_a(M)\rangle = \hat{U}_g^\dagger|\Psi_a(0)\rangle$, where $\hat{U}_g$ is a unitary operator accounting for the gauge transform between the LLL orbital bases before and after the Dehn twist (this unitary operator $\hat{U}_g$ will be defined in Sec. III B). This is for guaranteeing that the global phases randomly returned by numerical diagonalization are automatically canceled in Eq. (13), so that the obtained Berry phase is indeed gauge invariant. Moreover, when deciding the number of steps $M$, we require the wave-function overlap for two adjacent steps of the Dehn twist satisfying $|\langle\Psi_a(j+1)|\Psi_a(j)\rangle| > 0.99$ to insure that the deformation of the torus is performed adiabatically.

### B. Gauge Transformation

Now we derive the unitary operator $\hat{U}_g$ in Eq. (13), which connects the LLL orbital bases before and after the Dehn twist. Before the Dehn twist, the two elementary magnetic translational operators $\hat{t}_1 = \hat{t}(\frac{\vec{L}_1}{N_\phi})$ and $\hat{t}_2 = \hat{t}(\frac{\vec{L}_2}{N_\phi})$ on the rectangular torus satisfy $\hat{t}_1\hat{t}_2 = \hat{t}_2\hat{t}_1 e^{i\frac{2\pi N_p}{N_\phi}}$ and act on the single-particle orbital basis as[58,59]

$$\hat{t}_1|m\rangle = e^{i\frac{2\pi m}{N_\phi}}|m\rangle, \quad \hat{t}_2|m\rangle = |m+1\rangle, \tag{14}$$

where $m = 0, 1, \cdots, N_\phi - 1$ and $\hat{t}(\vec{r})$ is the general magnetic translational operator. After the Dehn twist, i.e., the $\mathcal{T}-$transformation, the orbital basis should be the same as the initial one up to a gauge phase $\gamma_m$, i.e., $\mathcal{T}|m\rangle = |\overline{m}\rangle = e^{i\gamma_m}|m\rangle$, where $|\overline{m}\rangle$ stands for the basis after the $\mathcal{T}-$transformation and satisfies

$$\hat{t}_1|\overline{m}\rangle = e^{i\frac{2\pi m}{N_\phi}}|\overline{m}\rangle, \quad \hat{t}\left(\frac{\vec{L}_1 + \vec{L}_2}{N_\phi}\right)|\overline{m}\rangle = |\overline{m+1}\rangle. \tag{15}$$

A combination of Eqs. (14) and (15) leads to $\gamma_{m+1} - \gamma_m = (2m+1)\frac{\pi}{N_\phi}$. Assuming $\gamma_m = Am^2 + Bm + C$, we get

$$\gamma_m = \pi\frac{m^2}{N_\phi} + C. \tag{16}$$

In the many-body level, the total gauge transform between the two equivalent orbital-basis Fock states before and after the Dehn twist is then simply given by

$$\hat{U}_g = \prod_{m\in\text{occupied}} e^{-i\gamma_m}|m\rangle\langle\bar{m}|, \tag{17}$$

where the sum is over all occupied orbitals[60].

An analytical derivation based on the real-space wave function of the orbital basis gives $C = 0$ in Eq. (16) (see Appendix Sec. A 2). However, we set $C = \gamma/N_p$ with $\gamma$ given by Eq. (10), which is equivalent to a gauge transform $|\Psi^\alpha;\tau+1\rangle \to e^{i\gamma}|\Psi^\alpha;\tau+1\rangle$. This choice is particularly convenient for numerical extractions of Hall viscosity, topological spin and central charge from the Dehn twist, because the non-universal part in the modular phase Eq. (8) is canceled by $CN_p$ such that the Berry phase Eq. (13) returned by numerical simulations only contains the pure geometric and topological terms.

## IV. RESULTS

### A. Flow of Energy Spectra

As an isolated ground-state manifold in the whole process of the geometric deformation is a requisite for a well defined

Berry phase, we first investigate the evolution of the low-energy spectra during the Dehn twist. Such an examination can reflect the stability of the FQH phase under the geometric deformation. Due to the relevance with realistic systems, we consider Coulomb interacting particles in what follows.

Remarkably, we observe an impressive robustness of Abelian FQH states against the Dehn twist. A typical example of $\nu = 1/2$ bosons is displayed in Fig. 2(a). Here we choose a geometric path from a rectangular to its equivalent one (as shown in Fig. 1). In this case, there is always a single ground state in the $(K_1, K_2) = (0, 0)$ momentum sector, which we confirm has a large overlap with the Laughlin state and never mixes with other excited levels as the twist angle $\theta$ of the torus changes during the Dehn twist. For each system size, the energy gap separating the ground state and excited states is almost constant during the Dehn twist even for the generic Coulomb interaction [Fig. 2(a)]. A finite-size scaling of the minimal energy gap $\Delta$ in the process of Dehn twist suggests that the gap is very likely to survive in the thermodynamic limit [Fig. 2(c)]. In addition, the minimum of the magnetoroton mode [at the bottom of excited levels in Fig. 2(a)] only changes a little with $\theta$, indicating that not only the ground state but also the low-energy excitations are stable against the Dehn twist.

We observe similar robustness of the ground-state manifold for other bosonic and fermionic Coulomb ground states at $\nu = 1/4, 1/3, 2/3$ and $2/5$, which correspond to the Abelian Laughlin, hierarchy, and Halperin states (see Appendix Sec. B). In all of these cases, the single ground state in the irreducible Brillouin zone evolves adiabatically and never mixes with excited levels during the Dehn twist. The energy gap is also expected to be finite, as indicated by the finite-size scaling of the minimal gap during the Dehn twist [Fig. 2(c)].

For non-Abelian FQH states, there are multiple ground states in the irreducible Brillouin zone, which makes the spectral flow more complicated. To pursue small finite-size effects in the Coulomb ground states, we focus on bosons at $\nu = 1$, where it has been confirmed that the Coulomb ground states are in the Moore-Read phase[61]. In this case, we again find remarkable robustness against the Dehn twist. Although the ground state in the $(K_1, K_2)$ sector evolves into the one in the $(K_1, K_1 + K_2)$ sector after the Dehn twist, the three ground states are always approximately degenerate and well separated from other excited levels by a finite energy gap [Fig. 2(c)] in the whole spectra flow [Fig. 2(b)].

### B. Berry phase and Hall viscosity

Let us now turn to discuss the accumulated Berry phase under the Dehn-twist operation. For specific $N_p$, $\nu$, $N_\phi = N_p/\nu$ and topological sector $a$, we first numerically calculate the Dehn-twist induced Berry phase at a fixed length $L = |\vec{L}_1|$ of the torus. We then vary $L$ around the square torus limit $L = \sqrt{2\pi N_\phi}$ to investigate the dependence of the Berry phase on $L$. We do these procedures in each topological sector $a$. Note that the torus area $|\vec{L}_1 \times \vec{L}_2| = 2\pi N_\phi$ is unchanged when we tune $L$.

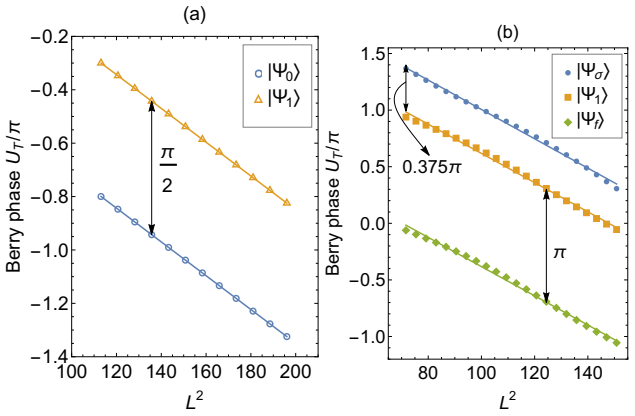


FIG. 3. **Accumulated Berry phase under Dehn-twist** $\vec{\tau} \to \vec{\tau} + \vec{e}_x$. Data are numerically calculated for Coulomb interacting bosons at (a) $\nu = 1/2$ and (b) $\nu = 1$, with $N_p = 12$ in both cases. Different topological sectors, with notations given in the main text, are distinguished by colors. Fitting each curve into Eq. (4) allows us to extract the guiding-center spin and topological spin in different topological sectors.

Remarkably, for various Abelian and non-Abelian FQH states that we have studied, the numerically obtained Berry phase $U_a^\mathcal{T}$ in each topological sector $a$ behaves nicely as a linear function of $L^2$ in the window of $L$ stated above (Fig. 3), which is consistent with the prediction of Eq. (4). Thus we expect that the slope of the linear function $U_a^\mathcal{T}(L^2)$ is given by the sector-independent guiding center Hall viscosity $\eta^g$ (as we have projected the Hamiltonian into a single Landau level, only the guiding-center part can be captured, see Appendix Sec. D), from which we can extract the guiding-center spin $s$ of the underlying phase. On the other hand, the sector-dependent topological spin $h_a$, describing the phase obtained by quasiparticle $a$ spinned by $2\pi$, and the chiral central charge $c$ are expected to be encoded in the intercept of $U_a^\mathcal{T}(L^2)$ in the limit of $L \to 0$. In particular, the difference between the intercepts of $U_a^\mathcal{T}(L^2)$ and $U_b^\mathcal{T}(L^2)$ should give us the topological spin difference $h_a - h_b$ between sectors $a$ and $b$.

For Abelian states, the ground states in different topological sectors can be distinguished by their momenta $(K_1, K_2)$, thus we straightforwardly have $|\Psi_a\rangle = |\Psi(K_1, K_2)\rangle$, where $|\Psi(K_1, K_2)\rangle$ is the ground state from numerical exact diagonalization. Based on this, we calculate the Berry phase $U_a^\mathcal{T}$, and indeed extract guiding center spin and sector-dependent topological spin that are very close to their theoretical values in pertinent FQH phases. For instance, we get $s \approx -0.4997$ for the two degenerate Coulomb ground states of bosons at $\nu = 1/2$ and the intercept difference gives $\Delta h \approx 0.2500$ [Fig. 3(a)]. This matches the $\nu = 1/2$ bosonic Laughlin state which carries $s = -1/2$ and has two types of quasiparticles with $h_0 = 0$ ($a = 0$ vacuum) and $h_\mathrm{s} = 1/4$ ($a = \mathrm{s}$ semion), respectively[41,53,62]. We have also explored other Abelian FQH states corresponding to the Laughlin states at $\nu = 1/3, 1/4$, hierarchy states at $\nu = 2/5, 2/3$, and Halperin states at $\nu = 2/3, 2/5$ (see Appendix Sec. B). We summarize these results in Tab. I, where all of the numerically extracted guiding center spin and topological spin are consistent with

TABLE I. In this table, we compare our numerical results with theoretical predictions. $s$ is the guiding-center spin, being related to the guiding-center Hall viscosity by $\eta^g = \frac{\hbar}{4\pi\ell^2}\frac{-s}{q}$. $h_a$ is the sector-dependent topological spin. See Appendix Sec. B for detailed information about the topological sectors of each FQH phase. Quantities with and without the superscript "cal" stand for numerically calculated results and theoretical values, respectively. We use parent Hamiltonians for the (221) and (332) Halperin states, otherwise we use the Coulomb interaction. N/A means no theoretical prediction on hand.

| | Laughlin | Laughlin | Laughlin | Hierarchy | Hierarchy | Moore-Read | Halperin (221) | Halperin (332) |
|---|---|---|---|---|---|---|---|---|
| $\nu = \frac{p}{q}$ | $\frac{1}{2}$ | $\frac{1}{3}$ | $\frac{1}{4}$ | $\frac{2}{5}$ | $\frac{2}{3}$ | $\frac{2}{2}$ | $\frac{2}{3}$ | $\frac{2}{5}$ |
| $s$ | $-\frac{1}{2}$ | $-1$ | $-\frac{3}{2}$ | $-3$ | $-2$ | $-1$ | $-1$ | $-2$ |
| $s^{\rm cal}$ | $-0.4997$ | $-0.9964$ | $-1.4469$ | $-2.9552$ | $-2.0840$ | $-1.0320, -1.0246$ | $-1.0499$ | $-2.0033$ |
| $h_a - h_0$ | $\frac{1}{4}$ | $\frac{1}{3}$ | $\frac{1}{8}, \frac{1}{2}$ | $N/A$ | $N/A$ | $\frac{1}{2}, \frac{3}{16}$ | $\frac{1}{3}$ | $\frac{1}{5}, \frac{2}{5}$ |
| $h_a^{\rm cal} - h_0^{\rm cal}$ | $0.2500$ | $0.3333$ | $0.1250, 0.5000$ | $0.2000, 0.4000$ | $0.3333$ | $0.5000, 0.1873$ | $0.3333$ | $0.2000, 0.4000$ |

theoretical predictions based on Jack polynomials or model wavefunction calculations[41].

For non-Abelian states, we need to appropriately superpose the ground states $|\Psi(K_1, K_2)\rangle$ obtained from numerical exact diagonalization to construct the state $|\Psi_a\rangle$ in a specific topological sector $a$. Here we take the $\nu = 1$ Coulomb interacting bosons in the Moore-Read phase as an example. In this case, the three numerical ground states are in the $(k_1, k_2) = (\pi, 0), (0, \pi)$ and $(\pi, \pi)$ momentum sectors. The Moore-Read phase has three types of quasiparticles: the vacuum $a = 0$, the fermionic anyon $a = f$ and the Ising anyon $a = \sigma$. In particular, the Ising anyon $\sigma$ carries non-Abelian braiding statistics which can lead to potential applications in topological quantum computation[63,64]. Based on the symmetry analysis, $|\Psi_a\rangle$ and $|\Psi(K_1, K_2)\rangle$ are related via $|\Psi_\sigma\rangle = |\Psi(0, \pi)\rangle$ and $|\Psi_{0,f}\rangle = \frac{1}{\sqrt{2}}(|\Psi(\pi, \pi)\rangle \pm e^{i\varphi}|\Psi(\pi, 0)\rangle)$, where $\varphi$ is chosen to guarantee that $|\Psi_0\rangle$ and $|\Psi_f\rangle$ are minimally entangled states[45,53,54] with respect to the bipartition of all $N_\phi$ Landau level orbitals (see Appendix Sec. E). Similar to the Abelian cases, we find that the Dehn-twist induced Berry phase of each such constructed $|\Psi_a\rangle$ also matches a linear dependence on $L^2$ for $L$ around the square torus limit [Fig. 3(b)]. The extracted guiding center spin is $s \approx -1.0320$ and $-1.0246$ for $|\Psi_\sigma\rangle$ and $|\Psi_{0,f}\rangle$, respectively, which is almost sector-independent and very close to the theoretical value $s = -1$ in the Moore-Read phase. The topological spin of $f$ and $\sigma$ are respectively determined by $h_f - h_0 \approx 0.5000$ and $h_\sigma - h_0 \approx 0.1873$, being consistent with expected "fermionic" and "Ising" statistics of quasiparticle $f$ and $\sigma$[65,66].

### C. Chiral central charge and edge physics

In the vacuum sector $a = 0$, the topological spin $h_a = 0$ such that the intercept of $U^{\mathcal{T}}_{a=0}(L^2)$ is solely contributed by the chiral central charge $c$. In this case, we can investigate the edge structure of an FQH state which is determined by $c$. As notable examples, we first consider the fermionic model Laughlin state at $\nu = 1/3$ and its particle-hole conjugate at $\nu = 2/3$. Working in the vacuum sector, we extract the central charge of the $\nu = 1/3$ model Laughlin state as $c \approx 1.01595$ (Fig. 4), which is close to the theoretical value $c = 1$ (see Appendix Sec. B for details). Physically, $c = 1$ means that the edge state is a single chiral bosonic field, being consistent with the well known edge structure of the $\nu = 1/3$ Laughlin state.

By contrast, there are multiple scenarios of the edge physics for the particle-hole conjugate of the $\nu = 1/3$ Laughlin state at $\nu = 2/3$. One possibility is that the edge current is carried by two chiral $\nu = 1/3$ edge modes[67,68]. However, it has been debated that the $\nu = 2/3$ state should harbor two counter-propagating $\nu = 1$ and $\nu = 1/3$ edge modes and edge reconstruction could occur in this hole-conjugate FQH state[69]. The difference between the two scenarios above is that the former hosts $c = 2$, while the latter has $c = 0$ due to the counter-propagating nature. As shown in Fig. 4, we obtain $c \approx 0.0159$ at $\nu = 2/3$ within very high accuracy. This result unambiguously points to the counter-propagating picture[69] and is also consistent with the recent shot noise measurements and other experiments[6,70,71]. In addition, we identify $c = 1$ for the model Halperin (333) state at $\nu = 1/3$ , which suggests its effective edge theory to be equivalent to the Laughlin $\nu = 1/3$ state. In this sense, our approach offers a guide to explore the edge physics of existing FQH effects.

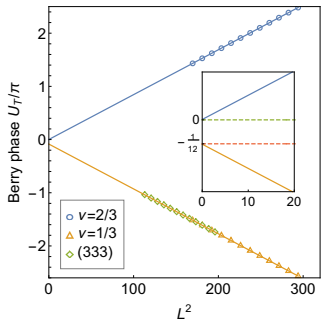


FIG. 4. **Chiral central charge.** Linear extrapolation of the Berry phase $U^{\mathcal{T}}_{a=0}(L^2)$ towards $L = 0$ for the model Laughlin state at $\nu = 1/3$ and its particle-hole conjugate at $\nu = 2/3$ in the vacuum sector $a = 0$. The intercept gives the chiral central charge $c \approx 1.0159$ for the model $\nu = 1/3$ Laughlin state and $c \approx 0.0159$ for its particle-hole conjugate at $\nu = 2/3$. Similarly, we identify $c \approx 0.9818$ for the model Halperin (333) state.

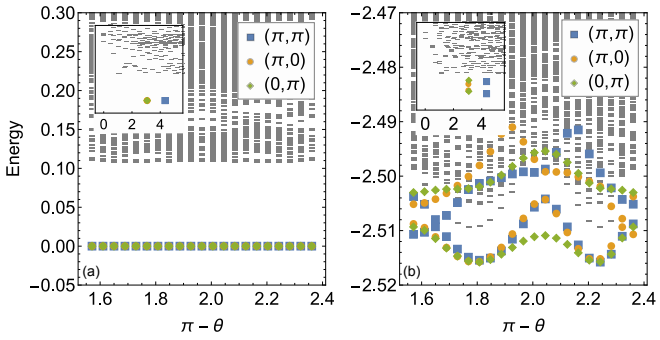


FIG. 5. **Energy spectra at $\nu = 5/2$.** The low-energy spectra of (a) the three-body parent Hamiltonian of the Pf state and (b) the two-body Coulomb interaction at $\nu = 1/2$ in the second Landau level as a function of the twist angle $\theta$ for $N_p = 12$ electrons. The lowest energy levels living in momentum sector $(0, \pi), (\pi, 0), (\pi, \pi)$ are labeled by colors. The insets show the energy spectra at $\theta = \pi/2$ as a function of $|\mathbf{K}|$.

## V. DISCUSSION

Apart from extracting geometric and topological quantum numbers of the underlying FQH state, our Dehn-twist approach also provides a distinctive viewpoint to inspect the stability of an FQH phase. In some cases such stability cannot be guaranteed by only studying finite-size samples with a fixed torus shape. Here we use the energy spectral flow under the Dehn twist as a criterion. As required by the gauge transformation, such an energy spectral flow is expected to maintain the ground-state degeneracy without level crossings with excited levels if the underlying FQH phase is really robust[5]. The results shown in Figs. 2(a) and 2(b) satisfy this requirement. However, we also notice a striking counterexample for Coulomb interacting electrons at $\nu = 5/2$ ($\nu = 1/2$ in the second Landau level). In this case, while the nature of the ground state is still under debate, there is one possibility that the ground-state manifold consists of the non-Abelian Pfaffian (Pf) and anti-Pfaffian (aPf) states that are degenerate in the thermodynamic limit[12,72–78]. As both the Pf and aPf states are three-fold degenerate in the irreducible Brillouin zone on the torus, the total ground-state degeneracy in the irreducible Brillouin zone is expected to be six-fold in this case. Some numerical attempts indeed reported the observation of six low-lying states at $\nu = 5/2$ on the torus of special shape[77,78]. However, we find that this feature is not stable under the Dehn twist. As shown in Fig. 5(b), while there are six low-lying states on the rectangular torus[77], three of them evolve into the higher-energy spectrum during the Dehn twist, making the Pf-aPf interpretation questionable. It is in sharp contrast to the case of the particle-hole symmetry breaking three-body parent Hamiltonian of the (anti-)Pfaffian state, for which the (anti-)Pfaffian state is always the zero-energy ground state regardless of the torus shape [Fig. 5(a)]. Moreover, Ref. 78 claimed that a quantum-well model with a finite layer-width could stabilize Pf and aPf states. Unfortunately, we observe similar level crossing with excited levels in the spectral flow of that model also. Thus, our calculations suggest that, compelling evidence on the torus geometry for Pf and aPf states at $\nu = 5/2$ is still far from conclusive (see discussion in Appendix Sec. B 5).

## VI. CONCLUSION AND OUTLOOK

In this work, we present a systematic scheme based on the Dehn-twist deformation on the torus geometry to identify the topological orders of fractional quantum Hall (FQH) liquids. With a gauge fixing procedure, we analytically derive the formula of the total Berry phase accumulated during the Dehn twist. This formula explicitly relates the geometric response of FQH liquids to their universal properties, such as the Hall viscosity, the topological spin, and the central charge of the edge conformal field theory. We then verify this formula in various microscopic models of Abelian and non-Abelian FQH liquids beyond model wave functions, demonstrating the potential of our scheme as a diagnosis of the topological order in a generic FQH state without prior knowledge. Motivated by the requirement of a well defined geometric Berry phase, we also suggest a separated ground-state manifold from excited levels in the whole process of geometric deformation as an indispensable criterion to justify the stability of an FQH phase.

Our approach opens up several future directions deserving further exploration. We mostly focus on FQH states in the lowest Landau level in this work. Considering that a series of FQH effects are also observed in higher Landau levels, we believe that our Dehn-twist protocol can shed light on the stability of those FQH states and their difference from the lowest-Landau-level FQH states from the aspect of geometric response. Moreover, in order to deepen our understanding of the interplay between topology and geometry, it is instructive to investigate how the geometric response of FQH liquids is affected by the breaking of the rotational invariance, such as in the cases of anisotropic FQH states[18,22] and FQH nematic phases[79,80]. Furthermore, it would be interesting to adjust our Dehn-twist protocol to lattice systems, such that it can be applied to the broad class of lattice topological states such as fractional Chern insulators[81–83].

## ACKNOWLEDGMENTS

D.L.H. and W.Z. thanks Tiansheng Zeng for simulating discussion, and Bo Yang, Chong Wang, and Jie Wang for helpful discussions. L.D.H. and W.Z. are supported by project 11974288 from NSFC and the foundation of Westlake University. Z.L. is supported by project 11974014 from NSFC. F.D.M.H is supported by DOE grant No. DE-SC0002140. D.N.S is supported by National Science Foundation Grants PREM DMR-1828019 and by the Princeton MRSEC through the National Science Foundation Grant DMR-1420541. The numerical calculations in this paper have been done on the supercomputing system in the Information Technology Center of Westlake University.

## Appendix A: Derivation of the Dehn-twist Berry phase for Abelian FQH states

In this section, we show a detailed derivation of the Dehn-twist induced Berry phase shown in the main text.

### 1. Lowest Landau level wave functions on the torus

The Hamiltonian of a charged particle on the torus spanned by $\vec{L}_1 = L\vec{e}_x$ and $\vec{L}_2 = L\vec{\tau}$ with a uniform perpendicular magnetic field can be written as

$$H_0(\mathbf{A},\tau) = \frac{1}{2}g^{ab}(\tau)D_a(\mathbf{A})D_b(\mathbf{A}), \tag{A1}$$

where

$$g(\tau) = \frac{1}{L^2\tau_2^2}\begin{pmatrix} |\tau|^2 & -\tau_1 \\ -\tau_1 & 1 \end{pmatrix}, \tag{A2}$$

and $D_a(\mathbf{A}) = -i\hbar\partial/\partial X^a + |e|A_a$ and $\mathbf{A} = (-\tau_2 L^2 B X^2, 0)$ are the covariant derivative and vector potential, respectively. The lowest Landau level (LLL) orbitals of Eq. (A1) are

$$\Psi_m(X^1, X^2|\tau) = \frac{1}{\sqrt{\pi^{1/2}L\ell}}\mathrm{e}^{i\pi N_\phi \tau [X^2]^2}\theta_{\frac{m}{N_\phi}}(N_\phi z/L|N_\phi\tau) \tag{A3}$$

with $m = 0, 1, \cdots, N_\phi - 1$, where $N_\phi = \frac{\vec{L}_1\times\vec{L}_2}{2\pi\ell^2} = \frac{\tau_2 L^2}{2\pi\ell^2}$ is the total flux through the torus, $\ell = \sqrt{\hbar/|e|B}$ is the magnetic length, $z = x+iy = L(X^1+\tau X^2)$ is the complex coordinate of electron, and $\theta_m(z|\tau)$ is the theta function defined as

$$\theta_\alpha(z|\tau) = \sum_{n\in Z}\exp\left(i\pi\tau(n+\alpha)^2 + i2\pi(n+\alpha)z\right). \tag{A4}$$

### 2. Dehn-twist transform of the LLL wave functions

Let us consider how the LLL wave functions evolve under the Dehn-twist transformation $\tau \to \tau+1$. After the Dehn twist, the coordinate $z = L(X^1+\tau X^2)$ can be rewritten as $z = L(X'^1+(\tau+1)X'^2)$. Thus we express the single-particle Hamiltonian in terms of $(X'^1, X'^2)$ as

$$H_0(\mathbf{A}',\tau+1) = \frac{1}{2}g^{ab}(\tau+1)D'_a(\mathbf{A}')D'_b(\mathbf{A}') \tag{A5}$$

with

$$g(\tau+1) = \frac{1}{L^2\tau_2^2}\begin{pmatrix} |\tau+1|^2 & -\tau_1-1 \\ -\tau_1-1 & 1 \end{pmatrix}, \tag{A6}$$

and the LLL wave function takes the form of

$$\Psi_m(X'^1, X'^2|\tau+1) = \frac{1}{\sqrt{\pi^{1/2}L\ell}}\mathrm{e}^{i\pi N_\phi(\tau+1)[X'^2]^2} \times\theta_{\frac{m}{N_\phi}}(N_\phi z/L|N_\phi(\tau+1)), \tag{A7}$$

where $D'_a(\mathbf{A}') = -i\hbar\partial/\partial X'^a + |e|A'_a$ and $\mathbf{A}' = (-\tau_2 L^2 B X'^2, 0)$ are the covariant derivative and vector potential in $(X'^1, X'^2)$, respectively. To compare Eq. (A7) with Eq. (A3), we need to write them in the same coordinate frame. Therefore, $H_0(\mathbf{A}',\tau+1)$ should be rewritten in $(X^1, X^2)$. By using relations

$$g(\tau+1) = \frac{1}{L^2\tau_2^2}\begin{pmatrix} 1 & -1 \\ 0 & 1 \end{pmatrix}g(\tau)\begin{pmatrix} 1 & 0 \\ -1 & 1 \end{pmatrix} \tag{A8}$$

and

$$\begin{pmatrix} D_1(\tilde{\mathbf{A}}) \\ D_2(\tilde{\mathbf{A}}) \end{pmatrix} = \begin{pmatrix} 1 & 0 \\ -1 & 1 \end{pmatrix}\begin{pmatrix} D'_1(\mathbf{A}') \\ D'_2(\mathbf{A}') \end{pmatrix} \tag{A9}$$

with $\tilde{\mathbf{A}} = (-\tau_2 L^2 B X'^2, \tau_2 L^2 B X'^2) = (-\tau_2 L^2 B X^2, \tau_2 L^2 B X^2)$, we find

$$H_0(\mathbf{A}',\tau+1) = H_0(\tilde{\mathbf{A}},\tau) = \frac{1}{2}g^{ab}(\tau)D_a(\tilde{\mathbf{A}})D_b(\tilde{\mathbf{A}}) \tag{A10}$$

with $D_a(\tilde{\mathbf{A}}) = -i\hbar\partial/\partial X^a + |e|\tilde{A}_a$. Because $D_a(\mathbf{A})$ and $D_a(\tilde{\mathbf{A}})$ can be related by a gauge transformation $\hat{\mathcal{U}} = \mathrm{e}^{-i\pi N_\phi [X^2]^2}$[46], i.e.,

$$D_a(\mathbf{A}) = \hat{\mathcal{U}}^\dagger D_a(\tilde{\mathbf{A}})\hat{\mathcal{U}}, \tag{A11}$$

we get

$$H_0(\mathbf{A},\tau) = \hat{\mathcal{U}}^\dagger H_0(\tilde{\mathbf{A}},\tau)\hat{\mathcal{U}}. \tag{A12}$$

Now we can see that the LLL wave function after the Dehn twist, when written in $(X^1, X^2)$, is

$$\hat{\mathcal{U}}\Psi_m(X'^1, X'^2|\tau+1) = \mathrm{e}^{i\pi\frac{m^2}{N_\phi}}\Psi_m(X^1, X^2|\tau), \tag{A13}$$

where we have used

$$\begin{aligned} &\theta_{\frac{m}{N_\phi}}(N_\phi z|N_\phi(\tau+1)) \\ &= \sum_n \mathrm{e}^{i\pi N_\phi\tau(n+\frac{m}{N_\phi})^2 + i2\pi(n+\frac{m}{N_\phi})N_\phi z + i\pi N_\phi(n+\frac{m}{N_\phi})^2} \\ &= e^{i\pi\frac{m^2}{N_\phi}}\sum_n(-1)^{nN_\phi}\mathrm{e}^{i\pi N_\phi\tau(n+\frac{m}{N_\phi})^2 + i2\pi(n+\frac{m}{N_\phi})N_\phi z} \\ &= e^{i\pi\frac{m^2}{N_\phi}}\theta_{\frac{m}{N_\phi}}(N_\phi z|N_\phi\tau). \end{aligned} \tag{A14}$$

Therefore, a phase factor $\mathrm{e}^{i\pi\frac{m^2}{N_\phi}}$ is gained in the $m$th LLL orbital after the Dehn twist. Note that Eq. (A13) is consistent with Eq. (16) in the main text.

### 3. FQH wave functions

We consider a multi-component FQH state whose wave function on the torus can be expressed in terms of the theta

function[40,46] (the single-component case can be reached by setting the number of component equal to one):

$$\Psi^{\boldsymbol{\alpha}}\left(\{z_i^I\}|\tau\right)=\mathcal{N}(\tau)f_c(\{Z^I\})f_r(\{z_i^I\}) \times\exp\left\{i\pi\tau N_\phi\sum_{I,i}\left(\frac{y_i^I}{L\tau_2}\right)^2\right\}, \tag{A15}$$

where $I$ is the index of component, $\boldsymbol{\alpha}$ is the vector labeling degenerate states, $z_i^I=L(X_i^{I1}+\tau X_i^{I2})$ is the coordinate of the $i$th particle in the $I$th component, and $Z^I=\sum_i z_i^I$ is the center-of-mass coordinate of the $I$th component. The relative part of the wave function is

$$f_r\left(\{z_i^I\}|\tau\right)=\left\{\prod_{I<J}\prod_{i,j}\eta^{-K_{IJ}}(\tau)\theta_{11}^{K_{IJ}}(z_i^I/L-z_j^J/L|\tau)\right\} \times\left\{\prod_{I}\prod_{i<j}\eta^{-K_{II}}(\tau)\theta_{11}^{K_{II}}(z_i^I/L-z_j^I/L|\tau)\right\}, \tag{A16}$$

where $K_{IJ}$ is the underlying $K$ matrix with dimension $\dim(K)=\kappa$ and diagonal elements $\boldsymbol{\kappa}=(K_{11},K_{22},\cdots,K_{\kappa\kappa})^T$, and

$$\theta_{11}(z|\tau)=\sum_{n\in\mathbb{Z}}\exp\left\{i\pi\tau(n+\frac{1}{2})^2+i2\pi(n+\frac{1}{2})(z+\frac{1}{2})\right\} \tag{A17}$$

is the odd Jacobi-theta function satisfying $\theta_{11}(-z|\tau)=-\theta_{11}(z|\tau)$. The center-of-mass part of the wave function is

$$f_c\left(\{Z^I\}|\tau\right)=\eta^{-\kappa}(\tau)f^{(\boldsymbol{\alpha},\boldsymbol{\eta})}(\boldsymbol{Z}/L|\tau) \tag{A18}$$

with

$$f^{(\boldsymbol{\alpha},\boldsymbol{\eta})}(\boldsymbol{Z}|\tau)=\sum_{\boldsymbol{n}\in\mathbb{Z}^\kappa}\exp\left\{i\pi(\boldsymbol{n}+\boldsymbol{\alpha}+\boldsymbol{\eta})^TK\tau(\boldsymbol{n}+\boldsymbol{\alpha}+\boldsymbol{\eta})\right\} \times\exp\left\{2\pi i(\boldsymbol{n}+\boldsymbol{\alpha}+\boldsymbol{\eta})^TK(\boldsymbol{Z}-\boldsymbol{\eta})\right\}, \tag{A19}$$

where $\boldsymbol{\eta}=K^{-1}\boldsymbol{\kappa}/2$ for fermions and $\boldsymbol{\eta}=\boldsymbol{0}$ for bosons, and $\boldsymbol{Z}=(Z^1,Z^2,\cdots,Z^\kappa)^T$. The normalization factor is

$$\mathcal{N}(\tau)=N_0\left[\sqrt{\tau_2}\eta(\tau)^2\right]^{\frac{1}{2}\boldsymbol{\kappa}^T\boldsymbol{N}}, \tag{A20}$$

where

$$\eta(\tau)=q^{1/24}\prod_{n=1}^{\infty}(1-q^n)|_{q=e^{i2\pi\tau}} \tag{A21}$$

is the $\tau$-dependent Dedekind's $\eta$-function, $\boldsymbol{N}=\left(N^1,N^2,\cdots,N^\kappa\right)^T$ with $N^I$ is the number of particles in the $I$th component, and $N_0$ is an area-dependent constant.

Now let us demonstrate how to get the vector $\boldsymbol{\alpha}$ in Eq. (A15). Note that $K\boldsymbol{\alpha}$ is the coset lattice $Z^\kappa/KZ^\kappa$ with only $|\det(K)|$ independent vectors, indicating $|\det(K)|$-fold degenerate on torus[9,40,84]. For the Laughlin $\nu=1/q$ state, its $K$ matrix is $K=q$ with coset lattice $Z/KZ=\{K\boldsymbol{\alpha}|0,1,\cdots,q-1\}$, corresponding to the $q$ degenerate states. For the Halperin $(mmn)$ state, its $K$ matrix is

$$K=\begin{pmatrix}m & n\\ n & m\end{pmatrix}$$

and its coset lattice is enclosed by the parallelogram spanned by two vectors $(m,n)$ and $(n,m)$, thus the number of independent vectors is equal to the area of the parallelogram, i.e. $|\det(K)|=m^2-n^2$. For instance, the coset lattice of the Halperin $(332)$ state is $Z^2/KZ^2=\{K\boldsymbol{\alpha}|(0,0),(1,1),(2,2),(3,3),(4,4)\}$. Once we get the coset lattice vector $K\boldsymbol{\alpha}$, the vector $\boldsymbol{\alpha}$ can be obtained by acting $K^{-1}$ on the left-hand side of $K\boldsymbol{\alpha}$. In this way, we have $\{\boldsymbol{\alpha}|0,1/q,\cdots,(q-1)/q\}$ for the Laughlin $\nu=1/q$ state and $\{\boldsymbol{\alpha}|(0,0),(1/5,1/5),(2/5,2/5),(3/5,3/5),(4/5,4/5)\}$ for the Halperin $(332)$ state.

#### 4. Dehn twist and modular information

Similar to the single-particle case, we introduce a many-body gauge transformation

$$\hat{\mathcal{U}}_g=\exp\left\{i\pi N_\phi\sum_{I,i}\left(\frac{y_i^I}{L\tau_2}\right)^2\right\} \tag{A22}$$

to relate the many-body wave functions before and after the modular transformation $\{\mathcal{T}:\tau\to\tau+1\}$. Using Eqs. (A15)-(A22), we can get

$$\begin{aligned}\hat{\mathcal{U}}_g\Psi^{\boldsymbol{\alpha}}\left(\{z_i^I\}|\tau+1\right)&=\hat{\mathcal{U}}_g\mathcal{N}(\tau+1)f_c(\{Z^I\}|\tau+1)f_r(\{z_i^I\}|\tau+1)\mathrm{e}^{-i\pi N_\phi(\tau+1)\sum_{I,i}\left(y_i^I/L\tau_2\right)^2}\\&=\mathcal{N}(\tau)f_c(\{Z^I\}|\tau)f_r(\{z_i^I\}|\tau)\mathrm{e}^{i\pi N_\phi\tau\sum_{I,i}\left(y_i^I/L\tau_2\right)^2}\mathrm{e}^{\frac{1}{12}i\pi(\boldsymbol{N}^TK\boldsymbol{N}-\kappa)}\mathrm{e}^{i2\pi h_{\boldsymbol{\alpha}}}\\&=\Psi^{\boldsymbol{\alpha}}\left(\{X_{I,i}^1,X_{I,i}^2\}|\tau\right)\mathrm{e}^{\frac{1}{12}i\pi(\boldsymbol{N}^TK\boldsymbol{N}-\kappa)}\mathrm{e}^{i2\pi h_{\boldsymbol{\alpha}}},\end{aligned} \tag{A23}$$

where we have used the following useful relations (here we assume the total flux $N_\phi$ through torus is even):

$$\begin{aligned}\eta(\tau+1) &= e^{i\pi/12}\eta(\tau),\\ \theta_{11}(z|\tau+1) &= e^{i\pi/4}\theta_{11}(z|\tau),\\ f^{(\boldsymbol{\alpha},0)}(\boldsymbol{Z}|\tau+1) &= e^{i\pi\boldsymbol{\alpha}^T K\boldsymbol{\alpha}} f^{(\boldsymbol{\alpha},0)}(\boldsymbol{Z}|\tau),\\ f^{(\boldsymbol{\alpha},K^{-1}\boldsymbol{\kappa}/2)}(\boldsymbol{Z}|\tau+1) &= e^{i\pi(\boldsymbol{\alpha}+\frac{1}{2}K^{-1}\boldsymbol{\kappa})^T K(\boldsymbol{\alpha}+\frac{1}{2}K^{-1}\boldsymbol{\kappa})}\\ &\quad\times f^{(\boldsymbol{\alpha},K^{-1}\boldsymbol{\kappa}/2)}(\boldsymbol{Z}|\tau).\end{aligned} \tag{A24}$$

Eq. (A23) immediately gives the matrix representation of the $\mathcal{T}$-transform as

$$\langle\Psi^{\boldsymbol{\beta}};\tau|\mathcal{T}|\Psi^{\boldsymbol{\alpha}};\tau\rangle = \delta_{\boldsymbol{\alpha}\boldsymbol{\beta}} \mathrm{e}^{i2\pi(h_{\boldsymbol{\alpha}}-\frac{c}{24})} \mathrm{e}^{\frac{1}{12}i\pi\boldsymbol{N}^T K\boldsymbol{N}}, \tag{A25}$$

where $c=\kappa$ is the chiral central charge of the underlying edge CFT and $h_{\boldsymbol{\alpha}}$ is the topological spin of the topological sector $\boldsymbol{\alpha}$ satisfying

$$\begin{aligned}h_{\boldsymbol{\alpha}} &= \frac{1}{2}\boldsymbol{\alpha}^T K\boldsymbol{\alpha}(\mathrm{mod}\ 1) \text{ for bosons}\\ h_{\boldsymbol{\alpha}} &= \frac{1}{2}(\boldsymbol{\alpha}+K^{-1}\boldsymbol{\kappa})^T K(\boldsymbol{\alpha}+K^{-1}\boldsymbol{\kappa}/2)(\mathrm{mod}\ 1) \text{ for fermions.}\end{aligned} \tag{A26}$$

### 5. Hall viscosity and geometric phase

Let us denote the wave function in Eq. (A15) as $\frac{1}{\sqrt{Z(\tau,\bar\tau)}}|\Phi;\tau\rangle$, where $\langle\{z_j^I\}|\Phi;\tau\rangle = N_0\eta(\tau)^{\boldsymbol{\kappa}^T\boldsymbol{N}} f_c(\{Z^I\}|\tau) f_r(\{z_i^I\}|\tau) e^{i\pi N_\phi\tau\sum_{I,i}\left(\frac{y_i^I}{L\tau_2}\right)^2}$, and $Z(\tau,\bar\tau)\equiv\langle\Phi;\tau|\Phi;\tau\rangle = \tau_2^{-\frac{1}{2}\boldsymbol{\kappa}^T\boldsymbol{N}} = \left(\frac{\tau-\bar\tau}{2i}\right)^{-\frac{1}{2}\boldsymbol{\kappa}^T\boldsymbol{N}}$ is a pure real part. Then we can calculate the Berry connection induced by the $\mathcal{T}$ deformation of the torus as[20,40]

$$\begin{aligned}\mathcal{A}_\tau &= i\langle\Psi;\bar\tau|\frac{1}{\sqrt{Z}}\partial_\tau\frac{1}{\sqrt{Z}}|\Psi;\tau\rangle = i\sqrt{Z}\partial_\tau\frac{1}{\sqrt{Z}} + \frac{i}{Z}\partial_\tau Z\\ &= \frac{i}{2}\partial_\tau\ln Z = -\frac{\boldsymbol{\kappa}^T\boldsymbol{N}}{8\tau_2},\\ \mathcal{A}_{\bar\tau} &= i\langle\Psi;\bar\tau|\frac{1}{\sqrt{Z}}\partial_{\bar\tau}\frac{1}{\sqrt{Z}}|\Psi;\tau\rangle = i\sqrt{Z}\partial_\tau\frac{1}{\sqrt{Z}}\\ &= -\frac{i}{2}\partial_{\bar\tau}\ln Z = -\frac{\boldsymbol{\kappa}^T\boldsymbol{N}}{8\tau_2}.\end{aligned} \tag{A27}$$

We can also rewrite Eq. (A27) in terms of $\mathcal{A}_{\tau_1}$ and $\mathcal{A}_{\tau_2}$:

$$\begin{aligned}\mathcal{A}_{\tau_1} &= \mathcal{A}_\tau + \mathcal{A}_{\bar\tau} = -\frac{\boldsymbol{\kappa}^T\boldsymbol{N}}{4\tau_2},\\ \mathcal{A}_{\tau_2} &= i\mathcal{A}_\tau - i\mathcal{A}_{\bar\tau} = 0.\end{aligned} \tag{A28}$$

So the corresponding Berry phase due to the geometric deformation of torus is[40,47]

$$\int_0^1 \mathcal{A}_{\tau_1}\mathrm{d}\tau_1 = -\frac{\boldsymbol{\kappa}^T\boldsymbol{N}}{4\tau_2} = -\hbar^{-1}\eta^H|L|^2. \tag{A29}$$

## Appendix B: More numerical results

In this section, we present more numerical results at various filling factors which are not shown in the main text. The path of Dehn twist is given in Fig. 1 in the main text.

### 1. Laughlin state

We first consider $\nu = 1/2$ bosons interacting via the Coulomb potential. In this case, the ground state should be described by the $\nu = 1/2$ Laughlin state. In Fig. 6(a), we show the low-energy spectrum as a function of momentum $K = \sqrt{K_1^2+K_2^2}$ for fixed geometric parameters $\theta = \pi/2$ and $\tau_2 = 1$ (symmetric rectangular). There is a single ground state in momentum sector $(0,0)$, which is separated from the excited levels by a finite energy gap. Considering the two-fold center-of-mass degeneracy at $\nu = p/q = 1/2$, we recover the two-fold ground-state degeneracy for the Laughlin $\nu = 1/2$ state. The magneto-roton branch above the ground state, representing the collective mode of quasiparticle-quasihole pair, can also be clearly seen in momentum sectors $K > 1$. We then vary the geometric parameter $\theta$ for a fixed system area $|\vec{L}_1\times\vec{L}_2|$. The ground state with momentum $(0,0)$ evolves adiabatically and never crosses with higher energy levels in the spectral flow [Fig. 6(b)]. By collecting the total Berry phase accumulated in the Dehn twist ($\tau\to\tau+1$) for different $L$, we get the plot of $U_\mathcal{T}$ versus $L^2$, as shown in Fig. 6(c). Fitting the numerically obtained $U_\mathcal{T}$ into the relation Eq. (4) in the main text, we get the guiding center spin as $s\approx -0.4997$ and topological spin as $h_1 - h_0 = 0.2500$ within machine precision, which are consistent with the theoretical predictions $s=-1/2$[41] and $h_1-h_0 = 1/4$[46] for the Laughlin $\nu = 1/2$ state. In particular, the topological spin $h_1-h_0 = 1/4$ signals that the elemental quasiparticle satisfies semionic statistics in which a semion goes back to itself by a self-rotation $8\pi$. The chiral central charge extracted in the vacuum sector converges to the theoretical value $c=1$ with the increasing of the system size [Fig. 6(d)].

The same analysis can be applied to Coulomb interacting bosons at $\nu = 1/4$, as shown in Fig. 7. In this case, there are four topologically distinct ground states captured by the $\nu = 1/4$ Laughlin states, labeled by their quasiparticle charges $Q = a/4$ (in unit of $e$) with $a = 0,1,2,3$. The different ground states can be distinguished by their topological spins, which we numerically extract as $h_{1(3)} - h_0 = 0.1250$ and $h_2 - h_0 = 0.5000$. These results indeed match the theoretical predictions for the $\nu = 1/4$ Laughlin state. Combining the $\nu = 1/2$ and $1/4$ results, we conclude that the quasiparticle $a$ in bosonic Laughlin $\nu = 1/q$ state ($q$ even integer) carries topological spin $h_a - h_0 = \frac{a^2}{2q}(\mathrm{mod}1)$. This expression is consistent with Eq. (A26).

For Coulomb interacting fermions at $\nu = 1/3$ whose ground state is described by the $\nu = 1/3$ Laughlin state, we get very similar results, as shown in Fig. 8. The obtained guiding center spin is $s\approx -0.9964$, which is very close to the theoretical prediction $s=-1$ from the Jack polynomial calcula-

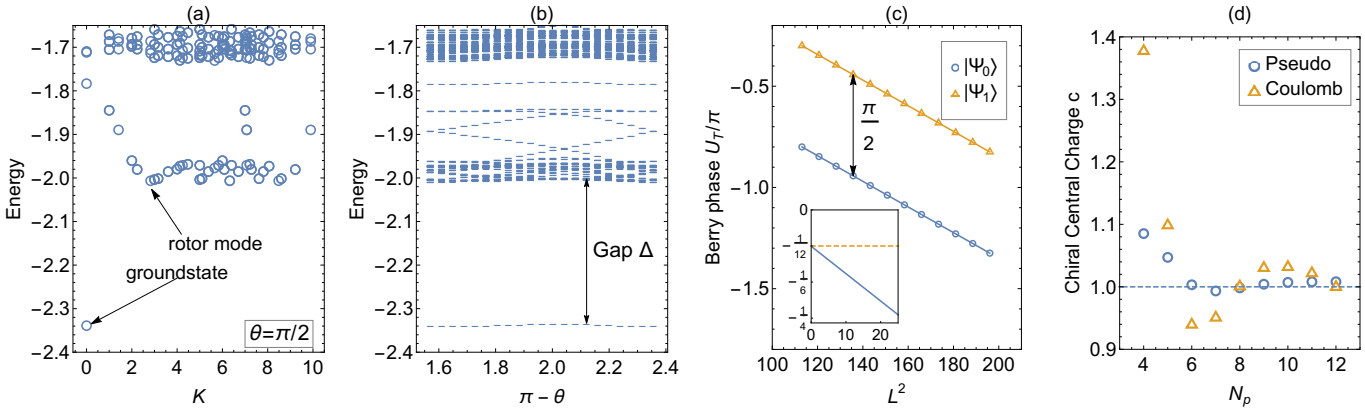


FIG. 6. **Numerical data for Coulomb interacting bosons at $\nu = 1/2$.** (a) The low-energy spectrum for geometric parameter $\theta = \pi/2$ and system size $N_p = 8$. (b) Flow of energy spectra with varying geometric parameter $\theta$. The energy gap (indicated by the arrow) is defined by the minimal difference between ground states and excited states in the whole process of Dehn twist. (c) Berry phase accumulated during the Dehn twist for the ground state $|\Psi_a\rangle$ of $N_p = 12$ in topological sector $a = 0, 1$. Here topological sectors are distinguished by their fractional quasiparticle charges $Q = a/2$ (in unit of $e$). Through the linear fitting against $L^2$, the obtained guiding center spin and topological spin are $s \approx -0.4997$ and $h_1 - h_0 = 0.2500$, respectively. The inset shows the intercept in the $a = 0$ sector, which returns the chiral central charge as $c \approx 0.9997$(the yellow dashed line is $-1/12$). (d) Chiral central charge $c$ for various system sizes $N_p$. The interaction in (d) is either the pseudopotential parent Hamiltonian of the $\nu = 1/2$ Laughlin state (blue circles) or the Coulomb potential (yellow triangles). The horizontal dashed line is $c = 1$.

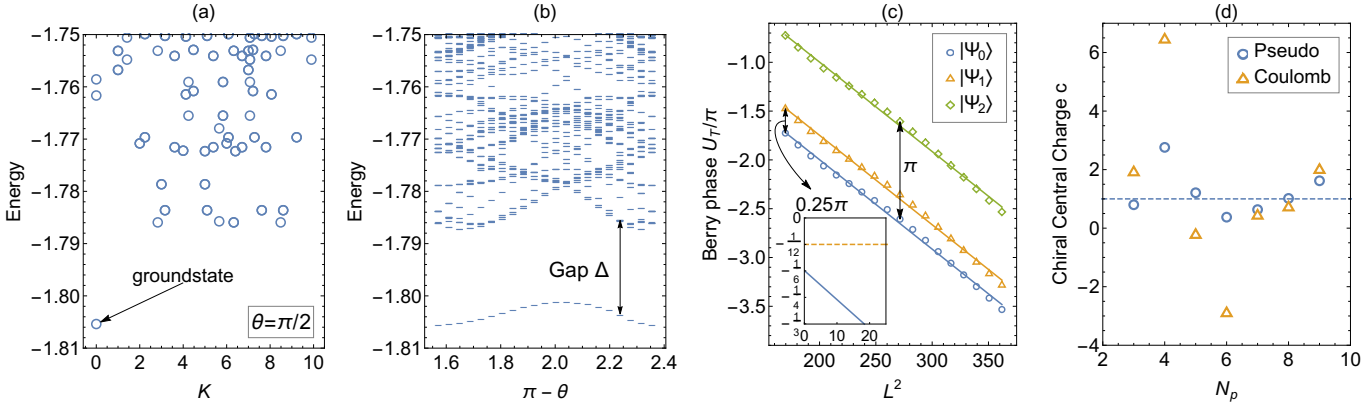


FIG. 7. **Numerical data for Coulomb interacting bosons at $\nu = 1/4$.** (a) The low-energy spectrum of $N_p = 8$ for fixed geometric parameters $\theta = \frac{\pi}{2}$ and $\tau_2 = 1$ (symmetric rectangular). The ground state is located in momentum sector $(0, 0)$. (b) Flow of energy spectra with varying geometric parameter $\theta$ for $N_p = 8$. (c) Berry phase accumulated during the Dehn twist for the ground state $|\Psi_a\rangle$ of $N_p = 9$ in topological sector $a = 0, 1, 2, 3$. $|\Psi_1\rangle$ and $|\Psi_3\rangle$ are equivalent. The obtained guiding center spin and topological spin are $s = -1.4469$ and $h_{1(3)} - h_0 = 0.1250, h_2 - h_0 = 0.5000$, respectively. The inset shows that the central charge $c$ has not converged for the largest system size $N_p = 9$ that we can reach. (d) Chiral central charge $c$ for various system sizes $N_p$. The interaction in (d) is either the pseudopotential parent Hamiltonian of the $\nu = 1/4$ Laughlin state (blue circles) or the Coulomb potential (yellow triangles). The horizontal dashed line is $c = 1$.

tion for the $\nu = 1/3$ Laughlin state[41]. According to Eq. (A26) and Ref. 46, the theoretical value of the topological spin of the $\nu = 1/3$ Laughlin state is $h_a = \frac{(a+q/2)^2}{2q} (\mathrm{mod} 1)$ in topological sector $a$ with quasiparticle charge $Q = a/3$ ($a = 0, 1, 2$), leading to $h_0 = 1/24 + 1/3 = 3/8, h_1 = h_2 = 1/24$. Indeed, we numerically obtain $h_0 - h_1 = h_0 - h_2 \approx 0.3333 = 1/3$ within machine precision. However, the Jack polynomial calculation in Ref. 41 on the cylinder geometry predicts $h_1 - h_0 = h_2 - h_0 = 1/6$. This discrepancy is due to the additional $\pi$ Berry phase for fermions on the torus geometry which we adopt, as noticed in Ref. 47.

### 2. Halperin state

Now we consider the two-component Halperin $(m, m, m-1)$ states at $\nu = 2/(2m-1) = p/q$[55]. For the fermionic (332) state, there are $|\det(K)| = 5$ degenerate ground states with $\{\boldsymbol{\alpha}|(0,0), (1/5,1/5), (2/5,2/5), (3/5,3/5), (4/5,4/5)\}$ (see Sec. A 3)[40,84]. Using Eq. (A26) we can obtain the theoretical values of the topological spin as $h_{0,0} = h_{2,2} = 9/20, h_{3,3} = h_{4,4} = 1/20, h_{1,1} = 1/4$, where the subscripts of $h$ correspond to the $K\boldsymbol{\alpha}$ values. Similarly, for the bosonic (221) state, there are $|\det(K)| = 3$ degenerate ground states with

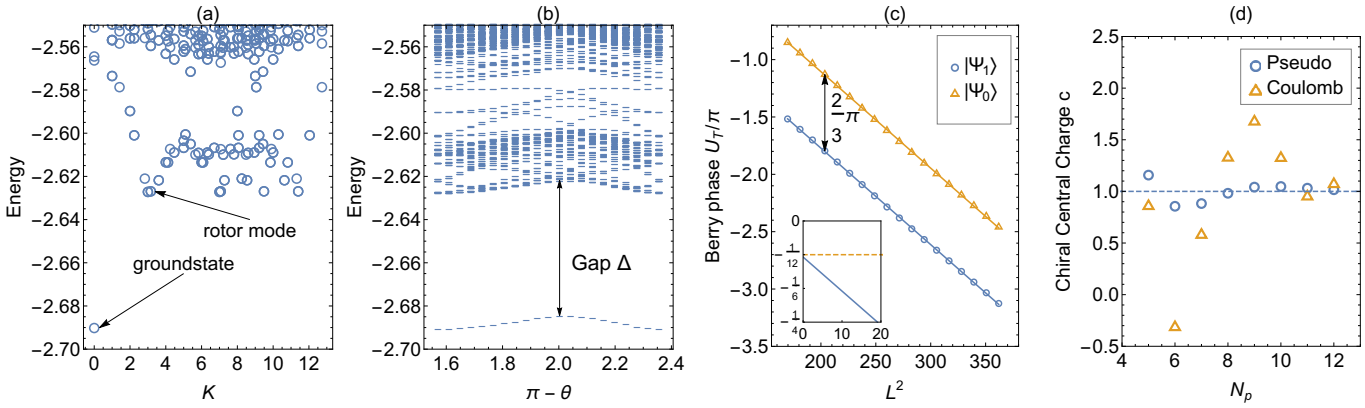


FIG. 8. **Numerical data for Coulomb interacting fermions at $\nu = 1/3$.** (a) The low-energy spectrum of $N_p = 10$ for fixed geometric parameters $\theta = \frac{\pi}{2}$ and $\tau_2 = 1$ (symmetric rectangular). The ground state is located in momentum sector $(0, 0)$. (b) Flow of energy spectra with varying geometric parameter $\theta$ for $N_p = 10$. (c) Berry phase accumulated during the Dehn twist for the ground state $|\Psi_a\rangle$ of $N_p = 12$ in topological sector $a = 0, 1, 2$. $|\Psi_1\rangle$ and $|\Psi_2\rangle$ are equivalent. The obtained guiding center spin and topological spin are $s \approx -0.9964$ and $h_0 - h_{1(2)} \approx 0.3333$, respectively. The inset shows that the intercept in the $a = 1(2)$ sector, which returns the chiral central charge as $c \approx 1.0699$ (the yellow dashed line is $-1/12$). (d) Chiral central charge $c$ for various system sizes $N_p$. The interaction in (d) is either the pseudopotential parent Hamiltonian of the $\nu = 1/3$ Laughlin state (blue circles) or the Coulomb potential (yellow triangles). The horizontal dashed line is $c = 1$.

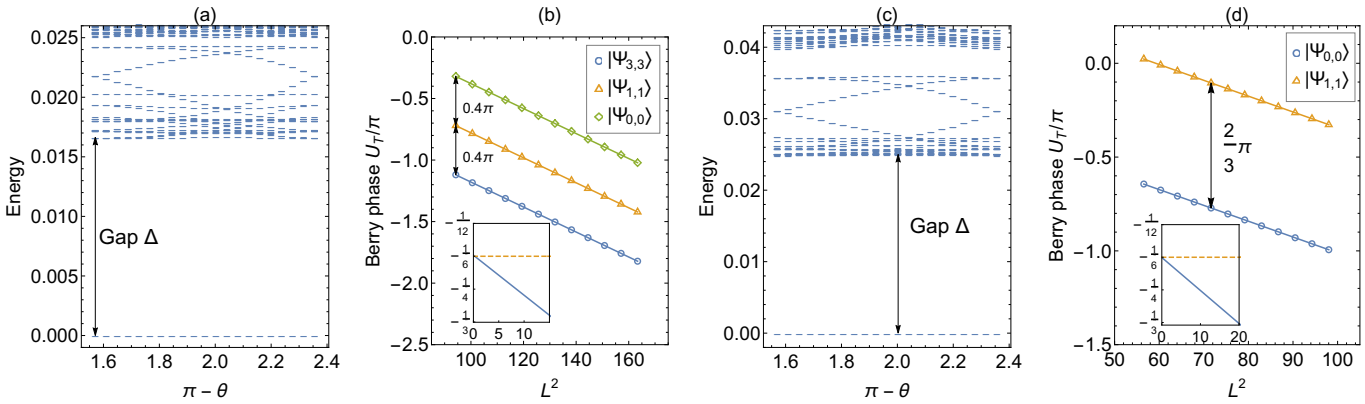


FIG. 9. **Numerical data for model Halperin states.** (a) Flow of energy spectra of the parent $(332)$ Hamiltonian with varying geometric parameter $\theta$ for $N_p = 8$ fermions. (b) Berry phase accumulated during the Dehn twist for the model $(332)$ state $|\Psi_{a,a}\rangle$ of $N_p = 8$ in topological sector $a = 0, 1, 3$. The obtained guiding center spin and topological spin are $s \approx -2.0033$ and $h_{0,0} - h_{1,1} = h_{2,2} - h_{1,1} = 0.2000$, $h_{1,1} - h_{3,3} = h_{1,1} - h_{4,4} = 0.2000$, respectively. The inset shows the intercept in the $a = 3$ sector, which returns the chiral central charge $c \approx 1.9678$ (the yellow dashed line is $-1/6$). (c) Flow of energy spectra of the parent $(221)$ Hamiltonian with varying geometric parameter $\theta$ for $N_p = 8$ bosons. (d) Berry phase accumulated during the Dehn twist for the model $(221)$ state $|\Psi_{a,a}\rangle$ of $N_p = 8$ in topological sector $a = 0, 1$. The obtained guiding center spin and topological spin are $s \approx -0.9986$ and $h_{1,1} - h_{0,0} = h_{2,2} - h_{0,0} = 0.3333$, repsectively. The inset shows that intercept in the $a = 0$ sector, which returns the chiral central charge $c \approx 2.0080$ (the yellow dashed line is $-1/6$).

$\{\boldsymbol{\alpha}|(0, 0), (1/3, 1/3), (2/3, 2/3)\}$, and the corresponding topological spins are $h_{0,0} = 0, h_{1,1} = h_{2,2} = 1/3$. Both the $(332)$ and $(221)$ states should have chiral central charge $c = 2$ because of their two-component nature. We numerically extract these topological indices of both the $(332)$ and $(221)$ states by diagonalizing their parent Hamiltonians, and the obtained numerical values indeed match theoretical predictions (Fig. 9).

### 3. Fermionic $\nu = 2/3$ state

Now we consider the particle-hole conjugate of the $\nu = 1/3$ Laughlin state, obtained by diagonalizing the parent Hamiltonian of the $\nu = 1/3$ Laughlin state, i.e., the first Haldane's pseudopotential[57]. The $K$ matrix of this state is[1]

$$K = \begin{pmatrix} 1 & 1 \\ 1 & -2 \end{pmatrix}, \tag{B1}$$

thus the degeneracy is three. According to Eq. (12) in Ref. 16, the theoretically predicted guiding center spin and topological spins of this state are $s = 1$ and $h_0 = -1/4, h_1 = h_2 =$

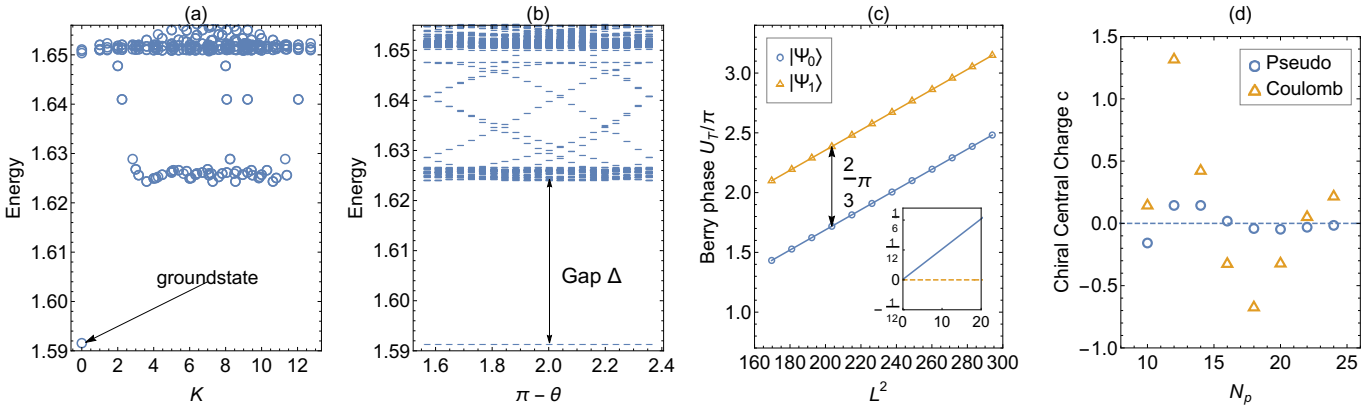


FIG. 10. **Numerical data for $\nu = 2/3$ fermions, interacting via the first Haldane's pseudopotential.** (a) The low-energy spectrum of $N_p = 20$ for fixed geometric parameters $\theta = \frac{\pi}{2}$ and $\tau_2 = 1$ (symmetric rectangular). The ground state is located in momentum sector $(0, 0)$. (b) Flow of energy spectra with varying geometric parameter $\theta$ for $N_p = 20$. (c) Berry phase accumulated during the Dehn twist for the ground state $|\Psi_a\rangle$ of $N_p = 24$ in topological sector $a = 0, 1$. The obtained guiding center spin and topological spin are $s \approx -0.9990$ and $h_{1(2)} - h_0 \approx 0.3333$, respectively. The inset shows the intercept in the $a = 0$ sector, which returns the chiral central charge as $c \approx 0.0160$ (the yellow dashed line is 0). (d) Chiral central charge $c$ for various system sizes $N_p$. The interaction in (d) is either the pseudopotential parent Hamiltonian of the $\nu = 1/3$ Laughlin state (blue circles) or the Coulomb potential (yellow triangles). The horizontal dashed line is $c = 0$.

$1/12$, respectively. Here the subscript of $h$ corresponds to the topological sector with quasiparticle charge $Q = a/3$ ($a = 0, 1, 2$). Indeed, we obtain numerical results $s \approx -0.9990$ and $h_{1(2)} - h_0 \approx 0.3333$, in excellent agreement with theoretical predictions (Fig. 10). Moreover, we extract the chiral central charge $c \approx 0.0160$ [Figs. 10(c),10(d)], which points to the counter-propagating edge modes. This is helpful for resolving the debate[67–69] about the edge structure of the $\nu = 2/3$ state (see the main text).

### 4. Hierarchy state

Starting from the Laughlin $\nu = 1/q$ state, quasiparticles can condensate into successive Laughlin states and generate a hierarchy of incompressible states. The most prominent state appears at $\nu = \frac{2}{5}$ for fermions and at $\nu = \frac{2}{3}$ for bosons, whose guiding center spins are $s = -3$ and $s = -2$, respectively.

Our numerical simulation gives $s \approx -2.0840$ for Coulomb interacting bosons at $\nu = 2/3$ and $s \approx -2.9552$ for Coulomb interacting fermions at $\nu = 2/5$, both of which match the above expected values (Fig. 11). Moreover, we also estimate the topological spins of elementary quasiparticles as $h_{1(2)} - h_0 \approx 0.3333 = 1/3$ for $\nu = 2/3$ bosons and $h_{1(4)} - h_0 \approx 0.2 = 1/5, h_{2(3)} - h_0 \approx 0.4 = 2/5$ for $\nu = 2/5$ fermions. The subscript $a$ of $h$ labels the topological sector with quasiparticle charge $Q = a/(2p+1)$ at $\nu = p/(2p+1)$ for fermions and $Q = a/(p+1)$ at $\nu = p/(p+1)$ for bosons.

### 5. Fermionic Moore-Read state

Despite that the FQH states at $\nu = p/q$ with odd $q$ can be understood by Laughlin's paradigm and further hierarchy theory or by Jain's composite fermion theory, the finding of even denominator $\nu = 5/2$ FQH state challenges our theoretical understanding of the FQH effect. Among multiple candidates, Pfaffian or anti-Pfaffian wave function proposed by Moore and Read[12,72,75] seems a promising candidate to describe the enigmatic nature of the $\nu = 5/2$ FQH effect. Although much efforts have been devoted to this long-standing issue[73,74,76–78,85], solid numerical evidence of topological ground-state degeneracy on the torus is still lacking. In the main text, we have shown that the quasi-degenerate ground states of pure Coulomb interaction are not stable against the Dehn twist transformation in finite systems. We notice that Ref. 78 proposed that the modified Coulomb interaction with a finite-layer width correction may enhance the Moore-Read signature in some range of aspect ratio of the torus. Here we investigate this possibility by using the modified Coulomb potential

$$V(k) = \frac{2\pi}{k} \frac{3kd + \frac{8\pi^2}{kd} - \frac{32\pi^4(1-e^{-kd})}{k^2d^2(k^2d^2+4\pi^2)}}{k^2d^2 + 4\pi^2} \tag{B2}$$

in an infinite square-well potential, where $d$ stands for the effective layer-width of the experimental GaAs quantum well structures. In our calculation, we set $d = 4\ell$ according to the discussion in Ref. 78. The low-energy spectrum at rectangular geometry is shown in Fig. 12(a), which exactly repeats the result in Fig. 4 of Ref. 78. The plausible six quasi-degenerate ground states are labeled by red circles. However, under the Dehn twist deformation, the six quasi-degenerate states evolve into higher levels, as shown in Fig. 12(b). Due to such level mixing, we cannot get the Hall viscosity and topological spin for the $\nu = 5/2$ Coulomb state even with a finite $d$. Here, our analysis based on geometric deformation suggests that numerical signature of the fermionic $\nu = 5/2$ Moore-Read state on the torus geometry is still questionable.

How to understand our results on the $\nu = 5/2$ FQH state? One possible understanding is that, the Coulomb ground states at $\nu = 5/2$ lie on the marginal boundary between Pfaffian and

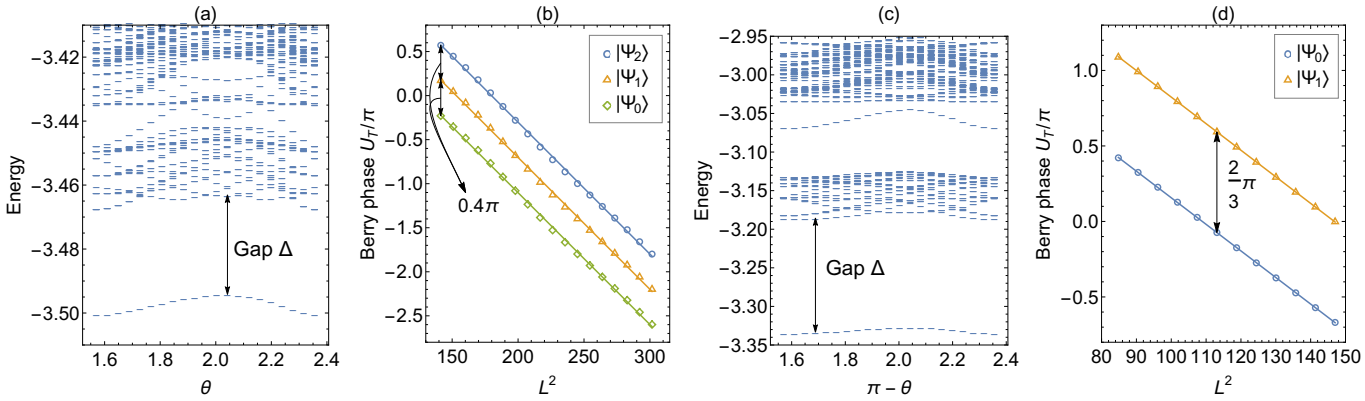


FIG. 11. **Numerical data for Coulomb interacting fermions at $\nu = 2/5$ and Coulomb interacting bosons at $\nu = 2/3$.** (a) Flow of energy spectra of $N_p = 12$ fermions at $\nu = 2/5$ with varying geometric parameter $\theta$. (b) Berry phase accumulated during the Dehn twist for the ground state $|\Psi_a\rangle$ of $N_p = 12$ fermions at $\nu = 2/5$ in topological sector $a = 0, 1, 2, 3, 4$. The obtained guiding center spin and topological spin are $s \approx -2.9552$ and $h_{1(4)} - h_0 = 0.2000$, $h_{2(3)} - h_0 = 0.4000$, respectively. (c) Flow of energy spectra $N_p = 12$ bosons at $\nu = 2/3$ with varying geometric parameter $\theta$. (d) Berry phase accumulated during the Dehn twist for the ground state $|\Psi_a\rangle$ of $N_p = 12$ bosons at $\nu = 2/3$ in topological sector $a = 0, 1, 2$. The obtained guiding center spin and topological spin are $s \approx -2.0840$ and $h_{1(2)} - h_0 = 0.3333$, respectively.

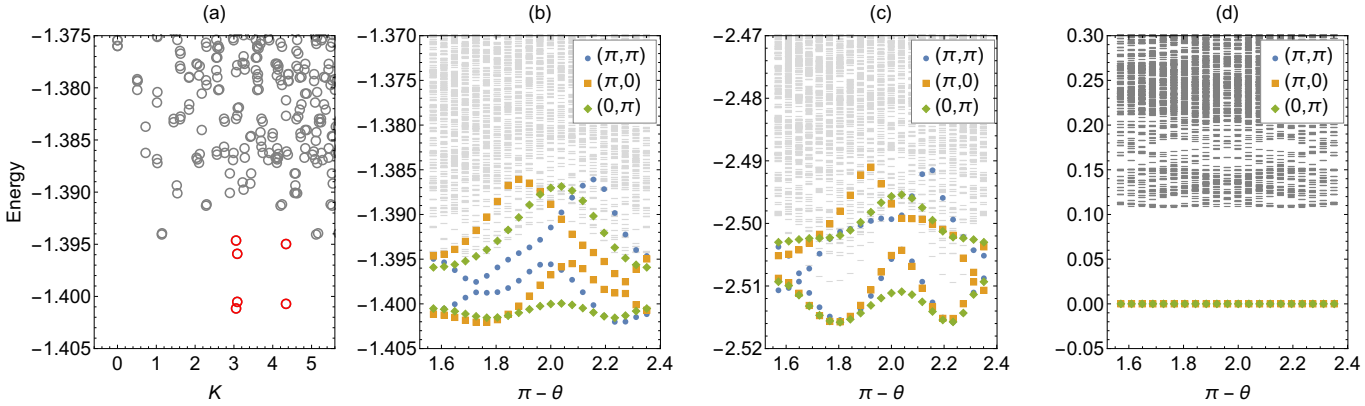


FIG. 12. (a) The low-energy spectrum of $N_p = 12$ fermions at $\nu = 5/2$ for $\theta = \frac{\pi}{2}$ and $\tau_2^{-1} = 0.99$[78]. The model contains a finite-layer width correction $d = 4\ell$ to the pure Coulomb interaction. The six quasi-degenerate ground states in momentum sectors $(\pi, 0), (0, \pi), (\pi, \pi)$ are indicated by red circles. (b) Flow of low-energy spectra with changing $\theta$. The ground states in momentum sectors $(\pi, \pi), (\pi, 0), (0, \pi)$ are labeled by blue circle, yellow square and green rhombus, respectively. (c) The low-energy spectrum of $N_p = 12$ fermions at $\nu = 5/2$ with the pure Coulomb interaction. (d) The low-energy spectrum of $N_p = 12$ fermions at $\nu = 5/2$ with the three-body parent Hamiltonian of the $\nu = 5/2$ fermionic Pfaffian state.

anti-Pfaffian states since the particle-hole symmetry cannot be broken by translational invariant two-body interactions on the torus[77]. The recent progresses of discovering non-Abelian statistics of the $\nu = 5/2$ FQH state on cylinder and sphere geometries may shed some light on this issue, where the particle-hole symmetry is broken spontaneously or explicitly[15,85,86]. In addition, recent thermal Hall measurement brings other possibilities to our attention. For example, the particle-hole symmetric Pfaffian state is proposed as a viable possibility[87]. The particle-hole Pfaffian state should host three-fold ground-state degeneracy (excluding the center-of-mass degeneracy). Unfortunately, in our extensive calculations (see Fig. 12), we did not observe any signal for the three-fold ground-state degeneracy either. In a word, our results call for further studies on the $\nu = 5/2$ problem on the torus geometry.

### 6. Bosonic Moore-Read State

In the main text, we have studied the Dehn twist of Coulomb interacting bosons at $\nu = 1$, whose ground state is described by the $\nu = 1$ bosonic Moore-Read state. Here, we do a similar study using the three-body parent Hamiltonian of the $\nu = 1$ bosonic Moore-Read state[88]. As shown in Fig. 13(a), the three degenerate $\nu = 1$ bosonic Moore-Read model states are the zero-energy ground states of this Hamiltonian. According to theoretical predictions, these three states correspond to three topological sectors: one with Abelian quasiparticle with topological spin $h_1 = 0$, one with Abelian quasiparticle with $h_f = \frac{1}{2}$, and one with non-Abelian quasiparticle (Ising anyon) with $h_\sigma = \frac{3}{16} = 0.1875$; and all of these three sectors should have the same guiding center spin

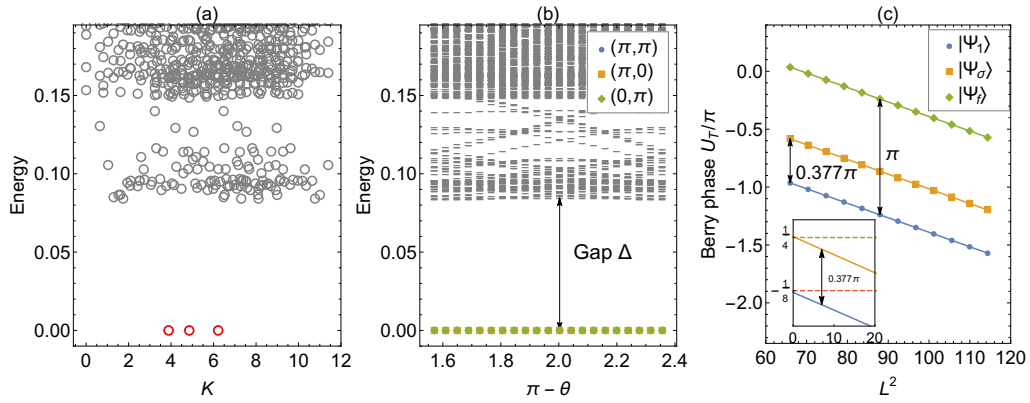


FIG. 13. **Numerical data for the model bosonic Moore-Read state at $\nu = 1$.** (a) The low-energy spectrum of the three-body parent Hamiltonian for $N_p = 12$, $\theta = \frac{\pi}{2}$, and $\tau_2 = 1.25$. The three degenerate ground states in momentum sectors $(\pi, 0), (0, \pi), (\pi, \pi)$ are indicated by red circles. (b) Flow of the low-energy spectra with changing $\theta$. The ground states in momentum sectors $(\pi, \pi), (\pi, 0), (0, \pi)$ are labeled by blue circle, yellow square and green rhombus, respectively. (c) Berry phase accumulated during the Dehn twist for the ground state $|\Psi_a\rangle$ of $N_p = 14$ in topological sector $a = 1, f, \sigma$. The obtained guiding center spin is $s \approx -1.0039(-0.9898)$ for $|\Psi_\sigma\rangle(|\Psi_1\rangle)$. The obtained topological spin is $h_f - h_1 \approx 0.5000$, $h_\sigma - h_1 \approx 0.1885$. The inset shows the intercepts in $a = 1$ and $a = \sigma$ sectors, leading to chiral central charge $c \approx 1.4276$ (the green dashed line is $-\frac{1}{8} + \frac{3}{8} = \frac{1}{4}$) for $a = \sigma$ and $c \approx 1.6441$ (the red dashed line is $-\frac{1}{8}$) for $a = 1$. The average $c$ over these two sectors is $c \approx 1.5359$.

$s = -1$. Indeed, in numerics we find guiding center spin and topological spins in good agreement with theoretical values [Fig. 13(c)]. In addition, the sector-averaged chiral central charge is determined to be $c \approx 1.5359$, close to the theoretical prediction $c = 3/2$. These facts form a compete diagnosis of the non-Abelian nature of the bosonic Moore-Read state at $\nu = 1$.

### Appendix C: Geometric Path Dependence

The topological information encoded in the Berry phase during the Dehn twist (see Sec. II C) is an intrinsic property of the underlying state, which should not depend on the specific Dehn-twist scheme that we choose. In the main text, we have considered the Dehn-twist from the rectangular torus to its equivalent one [Fig. 1(a)]. In the following, we will examine another Dehn-twist scheme, in which we deform the torus from a hexagon-like geometry to its equivalent one, i.e., $\theta$ is changed from $2\pi/3$ to $\pi/3$ [Fig. 14(a)].

The results of this different Dehn-twist scheme are shown in Fig. 14 for $\nu = 1/3$ Coulomb interacting fermions. On the initial symmetric hexagon geometry, the ground state is located in momentum sector $(0, 0)$, being separated from higher energy levels by a gap [Fig. 14(b)]. We also observe the magnetoroton mode above the ground state [Fig. 14(b)]. When the torus twist angle $\theta$ is changed from $2\pi/3$ to $\pi/3$, the energy gap isolating the ground state from excited levels keeps open [Fig. 14(c)]. We then calculate the Berry phase $U_a^{\mathcal{T}}$ accumulated in the ground state of topological sector $a$ during the geometric deformation. When analyzing the dependence of $U_a^{\mathcal{T}}$ on $L^2$, we use a different method from the one in the main text. Instead of only focusing on a single system size (the largest one we can reach numerically) and tuning $L$ near the square torus limit for this specific system size, here we consider various system sizes and fix $L$ – the length of $L_1$ as $L = \sqrt{2\pi N_\phi / \sin(2\pi/3)}$ for each system size. Then we can change $L$ and extract the dependence of $U_a^{\mathcal{T}}$ on $L^2$ by increasing the system size $N_\phi$. In Fig. 14(d), we show the Berry phase $U_{\mathcal{T}}$ for system sizes $N_p = 4, 6, 8, 10, 12$. Remarkably, the Berry phase again can be fitted into a linear function of $L^2$, which returns the guiding center spin as $s \approx -1.0119$ and the topological spin as $h_{1,2} - h_0 \approx 0.3333$. These values are consistent with the theoretical predictions and the previous numerical results obtained in Sec. B 1. Hence, we observe the same physics in two different schemes of Dehn twist and by two different methods of extracting the $L^2$-dependence in $U_a^{\mathcal{T}}$.

### Appendix D: Other topological quantities of FQH states

In our calculations, the total Hall viscosity is replaced by the guiding center Hall viscosity since we are working on the LLL-projected Hamiltonian. In fact, the total Hall viscosity of an FQH system should include two parts: the guiding center Hall viscosity $\eta^g$ and the Landau orbital Hall viscosity $\eta^o$. The guiding-center Hall viscosity $\eta^g$ describes an emergent geometric response of the correlated electrons, while the Landau-orbital Hall viscosity $\eta^o$ directly comes from the Landau-orbital form factor. The Landau-orbital Hall viscosity can be expressed in terms of the Landau-orbital spin $\tilde{s}$[19] as

$$\eta^o = \frac{\hbar}{4\pi\ell^2}\nu\tilde{s}, \tag{D1}$$

where the Landau-orbital spin $\tilde{s} = n + \frac{1}{2}$ for the $n$th Landau level. $\tilde{s}$ describes that, as the Landau level index increases, the orbital angular momentum carried by the cyclotron motion also increases. For a given filling factor $\nu$, both the Landau-orbital spin and Landau-orbit Hall viscosity are constant. Please note the Landau-orbital Hall viscosity exists even

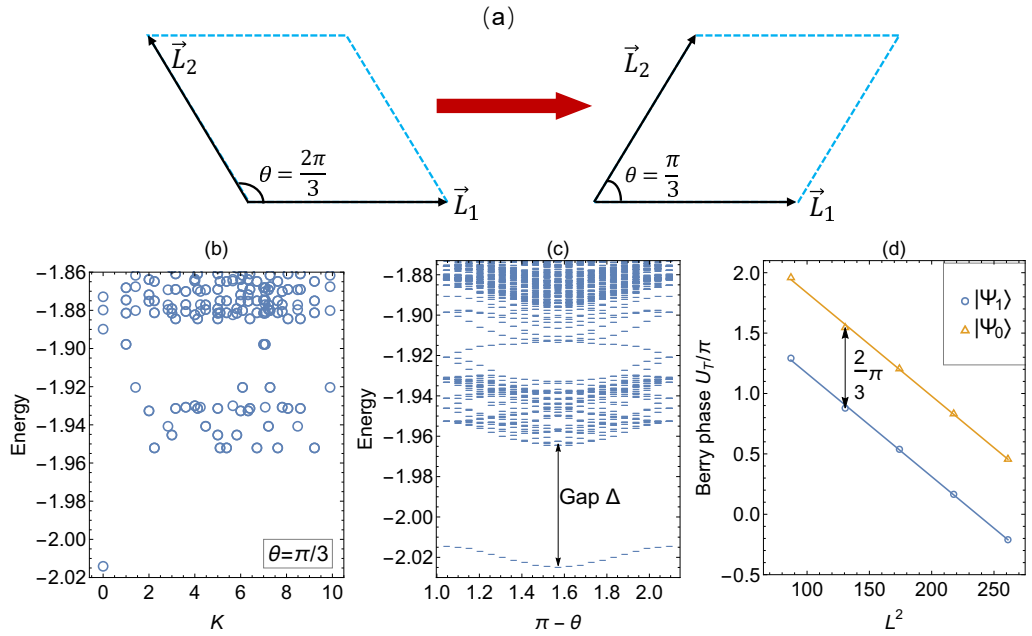


FIG. 14. (a) The Dehn-twist scheme that we use here is to deform the torus from a hexagon-like geometry to its equivalent one, i.e., $\theta$ is changed from $2\pi/3$ to $\pi/3$. (b) The low-energy spectrum for $N_p = 8$ Coulomb-interacting fermions at $\nu = 1/3$ on the symmetrical hexagonal geometry ($\theta = \frac{\pi}{3}$ and $\tau_2 = 1$). The ground state is located in the momentum sector $(0, 0)$. (c) Flow of energy spectra with varying geometric parameter $\theta$. (d) Berry phase accumulated during the Dehn twist for the ground state $|\Psi_a\rangle$, where $|\Psi_a\rangle$ is labeled by the fractional quasiparticle charge $Q = a/3$ (in unit of $e$) in topological sector $a = 0, 1, 2$. $|\Psi_1\rangle$ and $|\Psi_2\rangle$ are equivalent. Here $L$ is changed by fixing $L = \sqrt{2\pi N_\phi/\sin(2\pi/3)}$ for each system size then increasing $N_\phi$. The obtained guiding-center spin and topological spin are $s \approx -1.0119$ and $h_{1,2} - h_0 \approx 0.3333$, respectively.

when the particles are non-interacting.

Combining the the Landau-orbital and guiding-center Hall viscosities, we reach the total Hall viscosity

$$\eta^H = \eta^o + \eta^g = \frac{\hbar}{4\pi\ell^2}(\nu\tilde{s} - \frac{s}{q}) = \frac{\hbar\nu}{8\pi\ell^2}(2\overline{s}). \tag{D2}$$

Here we recover the so-called mean "orbital spin" defined by $\overline{s} = \tilde{s} - \frac{s}{p}$, which was first derived by Wen and Zee[16], and later by Read and Rezayi[20]. $\overline{s}$ can be further related to the topological shift $\mathcal{S}$ via $\mathcal{S} = 2\overline{s}$[20]. For a given FQH state, $\mathcal{S}$ is a topological number depending on the genus of the surface hosting the state. It always vanishes on the torus, but may take a nonzero value on the sphere. In the presence of $\mathcal{S}$, the number of particles and the number of flux is related by $N_\phi = N_p/\nu - \mathcal{S}$. Here, we see that $\mathcal{S}$ can be measured by the Dehn twist once we extract the guiding center spin $s$, even though the topological shift itself does not directly appear on the torus.

We close this section by illustrate some examples. For the $\nu = p/q = 1/q$ Laughlin state, the guiding center spin is $s = \frac{1}{2}(1-q)$. The mean orbital spin is then $\overline{s} = \tilde{s} - s/p = \frac{q}{2}$, where we choose $\tilde{s} = 1/2$ for the lowest Landau level. Therefore, the topological shift $\mathcal{S} = 2\overline{s} = q$. The same procedure can be easily adapted to obtain $\mathcal{S} = 4$ for the $\nu = 2/5$ fermionic hierarchy state, $\mathcal{S} = 3$ for the $\nu = 2/3$ bosonic hierarchy state, and $\mathcal{S} = 2$ for the $\nu = 1$ bosonic Moore-Read state.

## Appendix E: Minimally entangled state in the $\nu = 1$ bosonic Moore-Read manifold

We give a symmetry analysis of the $\nu = 1$ bosonic Moore-Read state based on its one-dimensional thin-torus limit. Due to $N_p = N_\phi$, the center-of-mass degeneracy is 1. The thin-torus limit of the $\nu = 1$ bosonic Moore-Read state has no more than two bosons in two consecutive LLL orbitals, thus there are three different thin-torus configurations[89]:

$$[20], \quad [02], \quad [11],$$

each of which can be adiabatically connected to the Moore-Read state with a definite type of quasiparticle (i.e., in a definite topological sector) when the torus deforms from the thin-torus limit to the two-dimensional limit. We label the corresponding Moore-Read quasiparticle eigenstates as $|20\rangle, |02\rangle$ and $|11\rangle$, which have different momenta: $|20\rangle$ and $|02\rangle$ have $K_1 = 1\%2$ (or $k_1 = \pi$), while $|11\rangle$ has $K_1 = 0\%2$ (or $k_1 = 0$).

Following the analysis in Ref. 59, we relate the quasiparticle eigenstates to the ground states $|k_1, k_2\rangle$ in the momentum sector $(K_1, K_2)$ by

$$\begin{aligned}
|02\rangle &= \frac{1}{\sqrt{2}}(|k_1 = \pi, k_2 = \pi\rangle + |k_1 = \pi, k_2 = 0\rangle), \\
|20\rangle &= \frac{1}{\sqrt{2}}(|k_1 = \pi, k_2 = \pi\rangle - |k_1 = \pi, k_2 = 0\rangle), \\
|11\rangle &= |k_1 = 0, k_2 = \pi\rangle.
\end{aligned} \tag{E1}$$

To see Eq. (E1) really represents the quasiparticle eigenstates, we provide two different proves here. One is that, we can construct the modular $\mathcal{S}$ matrix based on Eq. (E1). The other one is that, we can numerically prove that Eq. (E1) are the minimally entangled states in the Moore-Read manifold, which should be a faithful representation of quasiparticle eigenstates.

First, we relabel the quasiparticle eigenstates as $|\Xi_1^x\rangle = |02\rangle, |\Xi_2^x\rangle = |20\rangle$ and $|\Xi_3^x\rangle = |11\rangle$, and suppose that they are given by Eq. (E1). Under the $\mathcal{S}$ transformation, coordinates change according to $x \to y$ and $y \to -x$. In this case, the new set of quasiparticle eigenstates is

$$
\begin{aligned}
|\Xi_1^y\rangle &= \frac{1}{\sqrt{2}}(|k_1=\pi, k_2=\pi\rangle + |k_1=0, k_2=\pi\rangle) = \frac{1}{\sqrt{2}}[\frac{1}{\sqrt{2}}(|02\rangle + |20\rangle) + |11\rangle], \\
|\Xi_2^y\rangle &= \frac{1}{\sqrt{2}}(|k_1=\pi, k_2=\pi\rangle - |k_1=0, k_2=\pi\rangle) = \frac{1}{\sqrt{2}}[\frac{1}{\sqrt{2}}(|02\rangle + |20\rangle) - |11\rangle], \\
|\Xi_3^y\rangle &= |k_1=\pi, k_2=0\rangle = \frac{1}{\sqrt{2}}[|02\rangle - |20\rangle],
\end{aligned}
$$

since we apply a $\pi/2$ rotation

$$
\begin{aligned}
|k_1=\pi, k_2=\pi\rangle &\to |k_1=\pi, k_2=\pi\rangle \\
|k_1=0, k_2=\pi\rangle &\to |k_1=\pi, k_2=0\rangle \\
|k_1=\pi, k_2=0\rangle &\to |k_1=0, k_2=\pi\rangle
\end{aligned}
$$

on the ground states. Finally, we can get the modular $\mathcal{S}$ matrix as

$$
\mathcal{S} = \langle \Xi_i^x | \Xi_j^y \rangle = \frac{1}{2} \begin{pmatrix} 1 & 1 & \sqrt{2} \\ 1 & 1 & -\sqrt{2} \\ \sqrt{2} & -\sqrt{2} & 0 \end{pmatrix},
$$

which is exactly the theoretical prediction for the $\nu = 1$ bosonic Moore-Read state. Hence Eq. (E1) indeed gives the quasiparticle eigenstates.

In practice, since numerical diagonalization adds an additional phase to each $|k_1, k_2\rangle$, we must be careful when using Eq. (E1). Supposing that the numerically obtained ground state in the momentum sector $(k_1, k_2)$ for a fixed $\tau$ is $|k_1, k_2, \tau\rangle'$, we express the quasiparticle eigenstates as

$$
\begin{aligned}
|\Xi_1^x, \tau\rangle &= \frac{1}{\sqrt{2}}(|k_1=\pi, k_2=\pi, \tau\rangle' + e^{i\varphi}|k_1=\pi, k_2=0, \tau\rangle'), \\
|\Xi_2^x, \tau\rangle &= \frac{1}{\sqrt{2}}(|k_1=\pi, k_2=\pi, \tau\rangle' - e^{i\varphi}|k_1=\pi, k_2=0, \tau\rangle'), \\
|\Xi_3^x, \tau\rangle &= |k_1=0, k_2=\pi, \tau\rangle',
\end{aligned}
$$

where $\varphi$ depends on $\tau$ and is determined by minimizing the entanglement entropy for a half-half orbital bipartition of the whole system.

* zhuwei@westlake.edu.cn


[1] X.-G. Wen, "Quantum field theory of many-body systems: from the origin of sound to an origin of light and electrons," (2004).
[2] D. C. Tsui, H. L. Stormer, and A. C. Gossard, Phys. Rev. Lett. **48**, 1559 (1982).
[3] R. B. Laughlin, Phys. Rev. B **23**, 5632 (1981).
[4] D. J. Thouless, M. Kohmoto, M. P. Nightingale, and M. den Nijs, Phys. Rev. Lett. **49**, 405 (1982).
[5] Q. Niu, D. J. Thouless, and Y.-S. Wu, Phys. Rev. B **31**, 3372 (1985).
[6] A. Bid, N. Ofek, H. Inoue, M. Heiblum, C. Kane, V. Umansky, and D. Mahalu, Nature **466**, 585 (2010).
[7] M. Banerjee, M. Heiblum, A. Rosenblatt, Y. Oreg, D. E. Feldman, A. Stern, and V. Umansky, Nature **545**, 75 (2017).
[8] M. Banerjee, M. Heiblum, V. Umansky, D. E. Feldman, Y. Oreg, and A. Stern, Nature **559**, 205 (2018).
[9] X. G. Wen and Q. Niu, Phys. Rev. B **41**, 9377 (1990).
[10] R. B. Laughlin, Phys. Rev. Lett. **50**, 1395 (1983).
[11] D. Arovas, J. R. Schrieffer, and F. Wilczek, Phys. Rev. Lett. **53**, 722 (1984).
[12] G. Moore and N. Read, Nuclear Physics B **360**, 362 (1991).
[13] M. Levin and X.-G. Wen, Phys. Rev. Lett. **96**, 110405 (2006).
[14] A. Kitaev and J. Preskill, Phys. Rev. Lett. **96**, 110404 (2006).
[15] H. Li and F. D. M. Haldane, Phys. Rev. Lett. **101**, 010504 (2008).
[16] X. G. Wen and A. Zee, Phys. Rev. Lett. **69**, 953 (1992).
[17] F. Haldane, arXiv preprint arXiv:0906.1854 (2009).
[18] F. D. M. Haldane, Phys. Rev. Lett. **107**, 116801 (2011).
[19] J. E. Avron, R. Seiler, and P. G. Zograf, Phys. Rev. Lett. **75**, 697 (1995).
[20] N. Read, Phys. Rev. B **79**, 045308 (2009).
[21] C. Hoyos and D. T. Son, Phys. Rev. Lett. **108**, 066805 (2012).
[22] B. Yang, Z. Papić, E. H. Rezayi, R. N. Bhatt, and F. D. M. Haldane, Phys. Rev. B **85**, 165318 (2012).
[23] S. Johri, Z. Papić, P. Schmitteckert, R. N. Bhatt, and F. Haldane, New Journal of Physics **18**, 025011 (2016).
[24] T. Can, M. Laskin, and P. B. Wiegmann, Annals of Physics **362**, 752 (2015).
[25] S. Klevtsov and P. Wiegmann, Phys. Rev. Lett. **115**, 086801 (2015).
[26] T. Can, Y. H. Chiu, M. Laskin, and P. Wiegmann, Phys. Rev. Lett. **117**, 266803 (2016).
[27] T. Can and P. Wiegmann, Journal of Physics A: Mathematical and Theoretical **5**

[28] O. Saremi and D. T. Son, Journal of High Energy Physics **2012**, 91 (2012).
[29] D. T. Son, arXiv preprint arXiv:1306.0638 (2013).
[30] T. L. Hughes, R. G. Leigh, and O. Parrikar, Phys. Rev. D **88**, 025040 (2013).
[31] D. T. Son and C. Wu, Journal of High Energy Physics **2014**, 76 (2014).
[32] G. Y. Cho, Y. You, and E. Fradkin, Phys. Rev. B **90**, 115139 (2014).
[33] A. G. Abanov and A. Gromov, Phys. Rev. B **90**, 014435 (2014).
[34] A. Gromov and A. G. Abanov, Phys. Rev. Lett. **113**, 266802 (2014).
[35] A. Gromov, G. Y. Cho, Y. You, A. G. Abanov, and E. Fradkin, Phys. Rev. Lett. **114**, 016805 (2015).
[36] B. Bradlyn and N. Read, Phys. Rev. B **91**, 125303 (2015).
[37] A. Gromov and A. G. Abanov, Phys. Rev. Lett. **114**, 016802 (2015).
[38] T. Holder, R. Queiroz, and A. Stern, Phys. Rev. Lett. **123**, 106801 (2019).
[39] N. Read and E. H. Rezayi, Phys. Rev. B **84**, 085316 (2011).
[40] M. Fremling, T. H. Hansson, and J. Suorsa, Phys. Rev. B **89**, 125303 (2014).
[41] Y. Park and F. D. M. Haldane, Phys. Rev. B **90**, 045123 (2014).
[42] Y.-Z. You and M. Cheng, arXiv preprint arXiv:1502.03192 (2015).
[43] H. Moradi and X.-G. Wen, Phys. Rev. Lett. **115**, 036802 (2015).
[44] P. di Francesco, P. Mathieu, and D. Senechal, "Conformal field theory, corrected ed., ch. the o (n) model," (1999).
[45] Y. Zhang, T. Grover, A. Turner, M. Oshikawa, and A. Vishwanath, Phys. Rev. B **85**, 235151 (2012).
[46] X.-G. Wen, arXiv preprint arXiv:1212.5121 (2012).
[47] M. P. Zaletel, R. S. K. Mong, and F. Pollmann, Phys. Rev. Lett. **110**, 236801 (2013).
[48] H.-H. Tu, Y. Zhang, and X.-L. Qi, Phys. Rev. B **88**, 195412 (2013).
[49] There are two kinds of notations which we have used: one is the vector notation $\vec{\tau} = \tau_1\vec{e}_x + \tau_2\vec{e}_y$ and the other is the complex number notation $\tau = \tau_1 + i\tau_2$. They are equivalent and describe the same torus shape.
[50] T. Scaffidi, N. Nandi, B. Schmidt, A. P. Mackenzie, and J. E. Moore, Phys. Rev. Lett. **118**, 226601 (2017).
[51] A. Gromov and D. T. Son, Phys. Rev. X **7**, 041032 (2017).
[52] A. Gromov, S. D. Geraedts, and B. Bradlyn, Phys. Rev. Lett. **119**, 146602 (2017).
[53] W. Zhu, D. N. Sheng, and F. D. M. Haldane, Phys. Rev. B **88**, 035122 (2013).
[54] W. Zhu, S. S. Gong, F. D. M. Haldane, and D. N. Sheng, Phys. Rev. Lett. **112**, 096803 (2014).
[55] B. I. Halperin, Helv. Phys. Acta **56**, 75 (1983).
[56] We point out, the phase factor shown in Ref.[46] is incorrect, since the $\tau$-dependent factor $\mathcal{N}(\tau)$ is missing there.
[57] F. D. M. Haldane, Phys. Rev. Lett. **51**, 605 (1983).
[58] F. D. M. Haldane, Phys. Rev. Lett. **55**, 2095 (1985).
[59] B. A. Bernevig and N. Regnault, Phys. Rev. B **85**, 075128 (2012).
[60] The method that we used here is different from the one in Ref. 39. Ref. 39 computed the Berry field strength $\mathcal{F}$ by calculating the Berry flux through a small disk with radius $r$ in geometry space. In that method, the initial and final states are defined on identical torus geometry, so no gauge transformation is needed there. The accuracy of that method depends on the artificially selected radius $r$. For infinitely small values of $r$, that method is expected to give a good numerical estimation of $\mathcal{F}$. Two additional points further distinguish Ref. 39 from our study. First, Ref. 39 only considered rotationally invariant systems, such as the square torus geometry with $\theta = \pi/2$ and $L_1 = L_2$. Second, Ref. 39 worked on the model Hamiltonian constructed from Haldane pseudopotentials.
[61] Z. Liu, A. Vaezi, C. Repellin, and N. Regnault, Phys. Rev. B **93**, 085115 (2016).
[62] L. Cincio and G. Vidal, Phys. Rev. Lett. **110**, 067208 (2013).
[63] A. Kitaev, Annals of Physics **303**, 2 (2003).
[64] C. Nayak, S. H. Simon, A. Stern, M. Freedman, and S. Das Sarma, Rev. Mod. Phys. **80**, 1083 (2008).
[65] A. Kitaev, Annals of Physics **321**, 2 (2006), january Special Issue.
[66] W. Zhu, S. S. Gong, F. D. M. Haldane, and D. N. Sheng, Phys. Rev. B **92**, 165106 (2015).
[67] A. M. Chang and J. E. Cunningham, Phys. Rev. Lett. **69**, 2114 (1992).
[68] C. W. J. Beenakker, Phys. Rev. Lett. **64**, 216 (1990).
[69] C. L. Kane, M. P. A. Fisher, and J. Polchinski, Phys. Rev. Lett. **72**, 4129 (1994).
[70] H. Inoue, A. Grivnin, Y. Ronen, M. Heiblum, V. Umansky, and D. Mahalu, Nature Communications **5**, 4067 (2014).
[71] Y. Cohen, Y. Ronen, W. Yang, D. Banitt, J. Park, M. Heiblum, A. D. Mirlin, Y. Gefen, and V. Umansky, Nature Communications **10**, 1920 (2019).
[72] M. Greiter, X.-G. Wen, and F. Wilczek, Phys. Rev. Lett. **66**, 3205 (1991).
[73] R. H. Morf, Phys. Rev. Lett. **80**, 1505 (1998).
[74] E. H. Rezayi and F. D. M. Haldane, Phys. Rev. Lett. **84**, 4685 (2000).
[75] M. Levin, B. I. Halperin, and B. Rosenow, Phys. Rev. Lett. **99**, 236806 (2007).
[76] M. Storni, R. H. Morf, and S. Das Sarma, Phys. Rev. Lett. **104**, 076803 (2010).
[77] H. Wang, D. N. Sheng, and F. D. M. Haldane, Phys. Rev. B **80**, 241311 (2009).
[78] M. R. Peterson, T. Jolicoeur, and S. Das Sarma, Phys. Rev. Lett. **101**, 016807 (2008).
[79] Y. Liu, S. Hasdemir, M. Shayegan, L. N. Pfeiffer, K. W. West, and K. W. Baldwin, Phys. Rev. B **88**, 035307 (2013).
[80] N. Samkharadze, K. Schreiber, G. Gardner, M. Manfra, E. Fradkin, and G. Csáthy, Nature Physics **12**, 191 (2016).
[81] S. A. Parameswaran, R. Roy, and S. L. Sondhi, Comptes Rendus Physique **14**, 816 (2013).
[82] E. J. Bergholtz and Z. Liu, International Journal of Modern Physics B **27**, 1330017 (2013).
[83] T. Neupert, C. Chamon, T. Iadecola, L. H. Santos, and C. Mudry, Physica Scripta **2015**, 014005 (2015).
[84] E. Keski-Vakkuri and X.-G. Wen, International Journal of Modern Physics B **7**, 4227 (1993).
[85] K. Pakrouski, M. R. Peterson, T. Jolicoeur, V. W. Scarola, C. Nayak, and M. Troyer, Phys. Rev. X **5**, 021004 (2015).
[86] M. P. Zaletel, R. S. K. Mong, F. Pollmann, and E. H. Rezayi, Phys. Rev. B **91**, 045115 (2015).
[87] P. T. Zucker and D. E. Feldman, Phys. Rev. Lett. **117**, 096802 (2016).
[88] Z. Liu, E. J. Bergholtz, H. Fan, and A. M. Läuchli, Phys. Rev. B **85**, 045119 (2012).
[89] E. Ardonne, E. J. Bergholtz, J. Kailasvuori, and E. Wikberg, Journal of Statistical Mechanics: Theory and Experiment **2008**, P04016 (2008).